1990

Nonphotochemical hole burning and dispersive kinetics in amorphous solids

Michael Joseph Kenney
Iowa State University

Order Number 9110515

Nonphotochemical hole burning and dispersive kinetics in amorphous solids*

Kenney, Michael Joseph, Ph.D.

Iowa State University, 1990

U·M·I
300 N. Zeeb Rd.
Ann Arbor, MI 48106

Nonphotochemical hole burning and dispersive kinetics in amorphous solids

by

Michael Joseph Kenney

A Dissertation Submitted to the
Graduate Faculty in Partial Fulfillment of the
Requirements for the Degree of
DOCTOR OF PHILOSOPHY

Department: Chemistry
Major: Physical Chemistry

Approved:

Signature was redacted for privacy.

In Charge of Major Work

Signature was redacted for privacy.

For the Major Department

Signature was redacted for privacy.

For the Graduate College

Iowa State University
Ames, Iowa

1990

TABLE OF CONTENTS

PREFACE

The material presented in this report has been accepted for publication in Chemical Physics. The title of that report is "Dispersive kinetics of nonphotochemical hole growth for oxazine 720 in glycerol, polyvinyl alcohol and their deuterated analogues," and was authored by M. J. Kenney, R. Jankowiak and G. J. Small.

I. INTRODUCTION

Since 1972 [1, 2] the anomalous behaviors of the physical properties of glasses at very low temperatures have been the subject of many experimental and theoretical investigations [3, 4]. The properties include the specific heat (static and time-dependent), thermal conductivity, ultra-sound attenuation and, more recently, the pure dephasing and spectral diffusion of impurity electronic transitions [3-8]. It is generally believed that the anomalous behaviors are a manifestation of tunneling relaxation processes between bistable configurations of the glass which exist as a result of the structural disorder. Although simplistic, the TLS-model proposed by Anderson *et al.* [1] and Phillips [2] has proven remarkably successful in explaining the low temperature behaviors of a wide variety of properties. This model describes the tunneling in terms of a static distribution of asymmetric intermolecular double well potentials (two level systems or TLS) characterized by an asymmetry parameter (Δ) and tunnel parameter (λ). Ignorance of the microscopic structures of the TLS has led to considerable flexibility in the selection of phenomenological distribution functions for Δ and λ [9]. Two types of TLS are often considered: the intrinsic TLS

(TLS_{int}) of the "defectless" glass and the extrinsic TLS (TLS_{ext}) introduced by defects (impurities).

Nonphotochemical hole burning (NPHB) of impurity transitions in glasses is a striking example of phonon-assisted tunneling involving TLS_{ext} [10, 11]. The study of hole growth kinetics and spontaneous hole filling (a dark ground state process) are important approaches for the study of dispersive kinetics in glasses [12-18]. Persistent NPHB is a manifestation of the production of a post-burn impurity-glass configuration (following completion of the excitation cycle) which is thermally inaccessible to the pre-burn configuration at the burn temperature, T_B [5, 18]. The process is initiated by optical excitation of a narrow isochromat within the inhomogeneously broadened absorption profile of the impurity or probe molecule. It should be noted, however, that NPHB has recently been observed for delocalized exciton transitions [19] and vibrational bands of neat polymers [20].

The mechanism for NPHB proposed by Hayes and Small [21, 22] is based on the TLS_{ext} model. Bogner and Schwarz have proposed a similar model [23]. Each probe molecule has an associated TLS_{ext} which is labelled by α or β depending on whether the molecule is in its ground or excited state. In Fig. 1 the asymmetric double well potential shown is for TLS^{β}_{ext}. Optical excitation of its left-most well state is

Figure 1: Schematic of a two-level system (asymmetric intermolecular double well potential). The parameters are associated with TLS^{β}_{ext} (see text)

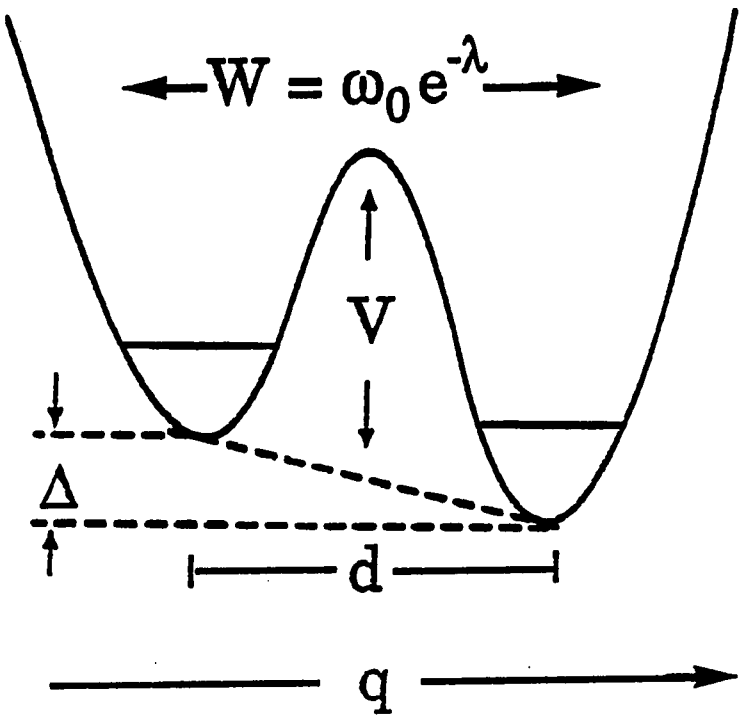
W = ω0 e-λ
V
Δ
d
q

viewed as originating from the corresponding well state of TLS^{α}_{ext} (not shown). Provided phonon-assisted tunneling is competitive with decay of state β, the asymmetry parameters (Δ) for TLS^{β}_{ext} and TLS^{α}_{ext} are different (in sign and/or magnitude) and tunneling relaxation in TLS^{α}_{ext} is slow on the time scale of the experiment, a mechanism for persistent hole production emerges.

Until recently this simple model, with its implied static distribution of asymmetry and tunnel parameters, appeared to be consistent with the available experimental data. However, based on detailed temperature dependent studies of cresyl violet in polyvinyl alcohol films, in which the entire hole profile (zero-phonon and phonon sideband holes and the antihole) was studied, Shu and Small have argued recently that the above model is inadequate [24]. They have proposed a model which is based on the hierarchy of constrained dynamical events which begins with rapid tunneling transitions of spatially extended (relatively delocalized) TLS_{int} triggered by optical excitation. These "outer-shell" relaxations are argued to result in an increase in the free volume of the probe-inner shell, which is viewed as a prerequisite for the tunneling step of hole formation. This model is consistent with the results presented in Refs. [23-29] and can explain, for example, why the antihole for $\pi\pi^*$ states of large organic

molecules (ranging from laser dyes to chlorophylls) is predominantly shifted to the blue of the burnt hole. However, the model retains the notion that the inherent disorder of the glass produces a distribution of values for the phonon-assisted tunneling relaxation frequency (R) associated with the relatively localized probe-inner shell coordinate which leads to hole formation.

In this paper, the results of an extensive study of the dispersive hole growth kinetics of Oxazine 720 (OX 720) in glycerol and polyvinyl alcohol (PVOH) hosts as well as their deuterated analogues are presented. Burn temperature dependent results are also presented which speak to the question of whether the distribution of hole burning efficiencies is dependent on temperature. The data for OX 720 in glycerol and PVOH are expansive in that they were produced with burn intensities which vary over three decades and fluences which vary over five decades. These and other results are theoretically analyzed using the distribution function, f(R), proposed by Jankowiak *et al.* [14, 30] and by Jankowiak and Small [18]. This function is based on the assumption that a Gaussian distribution for the tunnel parameter λ is physically reasonable [9, 31]. In all cases this distribution function is found to provide a satisfactory description of the dispersive kinetics. The linear electron-phonon coupling, which limits the saturated

depth of the zero-phonon hole, is taken into account in the analysis. In addition, an expression for the nonphotochemical hole burning quantum yield as a function of hole depth is presented.

II. EXPERIMENTAL

The probe molecule for the hole burning was Oxazine 720 perchlorate (see inset structure in Fig. 8) purchased from Exciton Chemical Co. The hydroxylated amorphous hosts used were glycerol and polyvinyl alcohol (PVOH, average molecular weight = 14,000) and their derivatives obtained by deuteration of the hydroxyl protons (deuterated glycerol > 98%, Merck, Sharp and Dohme; PVOD > 95%). PVOD films were prepared using a freeze-pump-thaw method [32-34] and film preparation has been described previously [35]. (It was found during these studies that the polymer solution could be easily "filtered" by centrifuging the liquid slurry for about 30 minutes prior to pouring the solution onto the glass plate. The resulting films were free of undissolved polymer and were, consequently, of better optical quality.)

Conversion of the PVOH films to PVOD was carried out under a dry nitrogen atmosphere and monitored via the -OH and -OD stretch modes in the infrared. (This method also enabled a determination of the film thickness due to the observed etalon effect.) Great care was taken to minimize exposure of the deuterated samples to air prior to their placement in the cryostat. For experiments with the perproto-hosts, exposure to air was not generally avoided

although one set of experiments was performed with dry glycerol. No significant differences in the dispersive hole growth kinetics were observed. Concentrations of the probe were in the range 10^{-5} - 10^{-6} M. The optical density (OD) at the burn wavelength was $\leq$ 0.4 for all but one sample studied. For OX 720 in glycerol two samples were studied with ODs of 0.6 and 0.3. No significant differences between the hole growth kinetics of these two samples were observed.

All experiments were performed at temperatures below 10 K using a Janis Research model 8-DT Super Vari-Temp cryostat. Temperatures were measured using a calibrated silicon diode temperature probe, Lake Shore Cryotronics model DT-500K. Glass samples were cooled quickly (< 10 min) to liquid helium temperatures. Polymer samples were rapidly immersed (< 1 min) to facilitate cooling reproducibility.

Hole growth kinetic studies were performed with a Coherent 699-21 ring dye laser pumped by a 5 W Ar^+ laser, Coherent Innova model 90-5. Optical elements of the dye laser comprised of a three plate birefringent (380 GHz band pass), an intra-cavity thin etalon (200 GHz free spectral range) and intra-cavity thick etalon (10 GHz free spectral range) provided a long term effective line width of < 20 MHz. Kinetics were monitored by continuous measurement of the intensity of the transmitted burn beam. See Fig. 2.

Figure 2: Schematic representation of hole burning apparatus

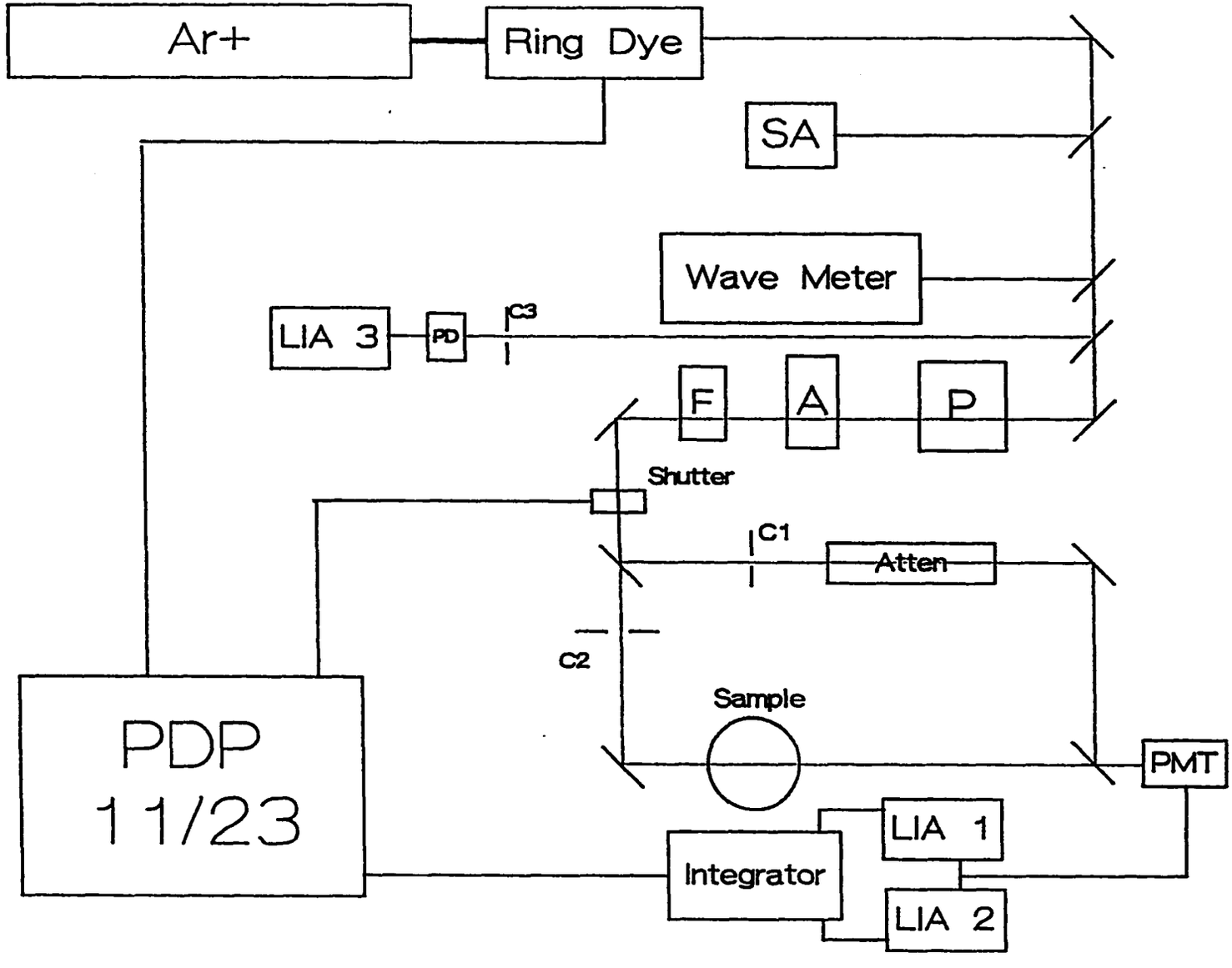
Ar+
Ring Dye
SA
Wave Meter
LIA 3
PD
C3
F
A
P
Shutter
C1
Atten
C2
Sample
PMT
PDP
11/23
Integrator
LIA 1
LIA 2

The optical density of the sample at the burn frequency (prior to burning) was measured using a home-built high resolution double beam spectrometer which has been described previously [35]. The double beam optical arms and electronics of this instrument (with two Laser Precision CTX-534 choppers operating at two different frequencies and two frequency referenced lock-in amplifiers, Ithaco model 397 EO) were also used as part of the zero-phonon hole (ZPH) kinetic analysis. Optical densities were measured as described in Ref. 35 and required that the ring dye laser output be shuttered while the output from the monochromator/arc lamp combination was unblocked. The addition of a movable mirror just after the monochromator facilitated this procedure. See Ref. 35 for the exact location.

Prior to burning, the relative intensities of the laser beam in the sample and reference arms of the double beam set-up were adjusted to provide the correct optical density of the sample. The intensity of the sample arm was attenuated due to reflections off the windows on the cryostat and due to the sample being present in the beam. The reference arm was attenuated in order to compensate for these losses through the use of an NRC model 935-5 variable attenuator. The laser intensity was decreased significantly during this procedure in order to avoid hole burning. Pre-

burn scans were generally made to ensure that no hole had been produced during the alignment.

Hole burning was initiated and terminated through computer control of the shutter. Subsequent to kinetic analyses, hole profiles were measured with picowatt probe intensity in order to determine that phonon sideband hole structure was not interfering with the zero-phonon hole at the burn frequency. The profiles were obtained by scanning over the 30 GHz spectral range of the laser. During hole growth, the laser frequency was fixed at the center of the scan window. Both operations were controlled through the computer, see Appendix B.

Due to laser instability at the edges of the scan window, frequency scans were usually made over a 25 GHz range symmetric about the burn frequency. Careful alignment of the laser was needed to ensure stability over the scan region. If the laser was misaligned or had drifted during prolonged use it tended to hop between modes and was unsuitable for spectral analysis. In the event of a mode hop, observed as a discontinuity in the output from the spectrum analyzer (SA in Fig. 2), the spectral scan was repeated or the laser was "tweaked" slightly to adjust for minor misalignments. The spectrum resulting from a laser mode hop provided the desired information regarding the spectral baseline but was unsuitable for publication.

Burn intensities were measured using a photodiode in combination with a lock-in amplifier that was referenced to a Coherent model 210 power meter. The output intensity of the ring dye laser was attenuated using an NRC model 935-3 variable attenuator in combination with an optical polarizer. This intensity was measured using the Coherent model 210 power meter and an "equivalent" output was measured using the photodiode/lock-in amplifier combination. A measure of the intensity at the sample position was then made using the photodiode. The ratio of the intensity at the sample position and at the position of the power meter enabled a determination of the sample intensity to within ~ 20%.

Subsequent attenuations were obtained using neutral density filters. The output from the ring dye laser was continuously monitored using the photodiode/lock-in combination. This arrangement provided power densities of 5 nW/cm^2 to 1000 nW/cm^2. Laser stability, measured using a Spectra-Physics model 470-04 confocal spectrum analyzer, was also monitored continuously.

For the analysis of hole growth kinetics at 1.6 K a value for the peak absorption cross-section, σ, for the zero-phonon line (ZPL) is required. Uncertainty in its determination stems mainly from the uncertainty in the homogeneous width of the ZPL at 1.6 K. Hole burning

measurements have yielded a homogeneous line width of 250 MHz for these systems. See Fig. 3. This value was used for the calculations of σ which are now presented. Two approaches were utilized. The first involves the calculation of the 0X 720 transition dipole length from the measured fluorescence decay constant, 3.7×10^{-8} s^{-1} [36]. The dipole length is 3.8 Å. This value was then used in the standard quantum mechanical expression for σ. The value obtained is $\sigma = 2 \times 10^{-10}$ cm^2 for the transition dipole parallel to the electric field vector of the light field and a refractive index of 1.5. However, this value for σ is apportioned between the origin and vibronic absorption transitions. From low temperature absorption spectra an estimate for a Franck-Condon factor of 0.3 for the origin band of interest is made. In addition there is a Franck-Condon factor associated with the matrix phonons. In the Results section experimental data are used to determine a value of 0.65 for this factor. With these two Franck-Condon factors the peak absorption cross-section for the ZPL of the zero-vibron level is $\approx 40 \times 10^{-12}$ cm^2 at 1.6 K. The second approach, scales the measured room temperature value for σ of the origin band, 3.6×10^{-16} cm^2, by the ratio of the 1.6 K homogeneous linewidth to the room temperature homogeneous line width. With an estimate for the room temperature homogeneous line width of 500 cm^{-1}, the scaled value for σ at

Figure 3: Constant burn intensity study of Oxazine 720 in polyvinyl alcohol. Conditions: I_B = 27 nW/cm^2, $T_B = T_R$ = 1.6 K and ω_B = 15408 cm^{-1}. Extrapolation to zero burn time gives a FWHM of 500 MHz which corresponds to Γ_{hom} = 250 MHz

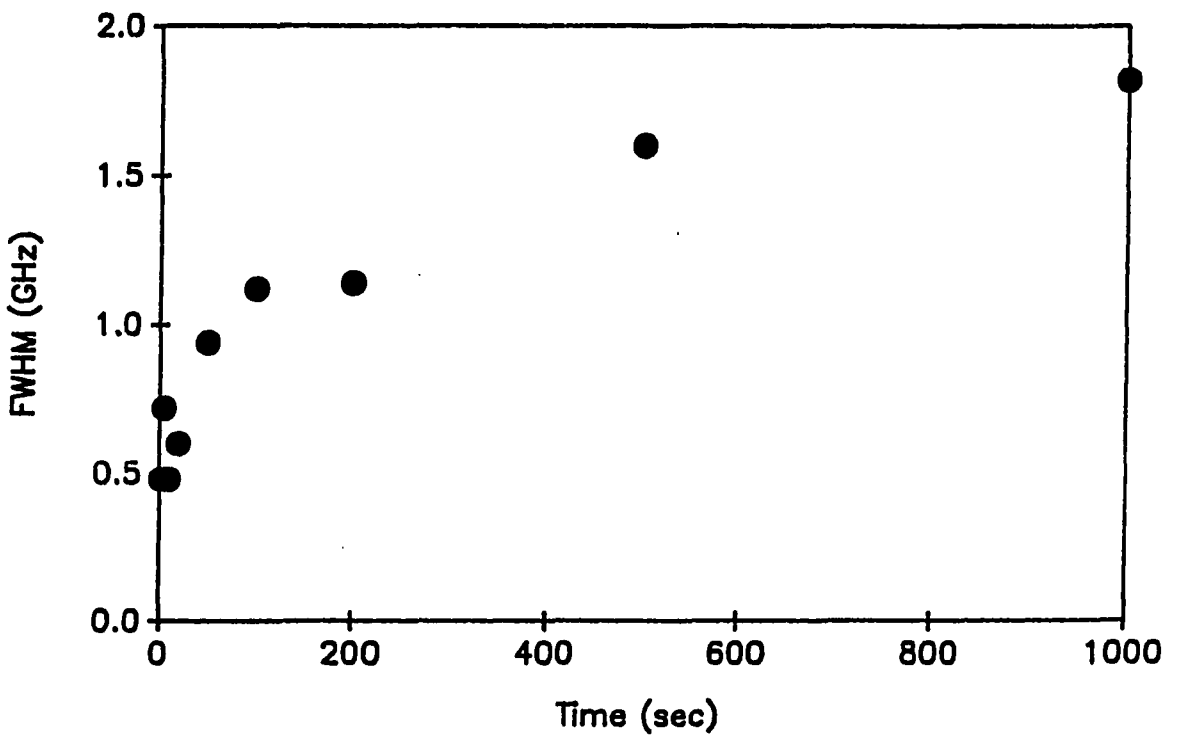
2.0
1.5
1.0
0.5
0.0
FWHM (GHz)
0
200
400
600
800
1000
Time (sec)

1.6 K is 14 x 10^{-12} cm^2 when the phonon Franck-Condon factor is taken into account. However, this value must be multiplied by a factor of 3 to obtain σ for the case where the transition dipole is parallel to the polarization vector (since the room temperature σ value was obtained for a randomly oriented sample). Thus, these two approaches yield about the same value for σ, $\approx$ 40 x 10^{-12} cm^2.

Based on photon echo and hole burning measurements on resorufin in alcohol glasses, Fayer and his group have recently concluded that hole burning overestimates the homogeneous line width at low temperatures, e.g., by a factor of 4 at 1.6 K and that this is a consequence of slow spectral diffusion processes [7, 37, 38]. Although this conclusion has been somewhat controversial [39], it is considered quite reasonable. The simulations presented here were obtained with $\sigma \approx 40 \times 10^{-12}$ cm^2. It will be shown, however, that an increase in this value to 160 x 10^{-12} cm^2 only increases the value for the mean tunnel parameter obtained with $\sigma = 40 \times 10^{-12}$ cm^2 by $\lesssim$ 10%.

III. THEORY

An expression, D(t), is derived in this section which will be used to describe the dispersive kinetics of nonphotochemical zero-phonon hole growth for OX 720 in glycerol and PVOH. As discussed in the Introduction, the mechanism for NPHB recently proposed by Shu and Small [24] retains an essential idea of the earlier model [21, 22]. It is that the rate determining step for hole formation is phonon-assisted tunneling of TLS_{ext}^{β} (β denotes the impurity excited electronic state) and that the intrinsic disorder of the glass leads to a distribution of tunneling frequencies. However, the new model asserts that the tunneling is strongly biased towards processes that involve phonon emission [24]. That is, the excited state energy (as well as the ground state) of the probe molecule for the post-burn configuration is lower than that for the pre-burn configuration. The excited state energy difference will be denoted by E. For a single TLS_{ext}^{β} the downward phonon assisted relaxation rate is [3, 5]

$$R = (3f^2W^2E/16\pi\rho c^5\hbar^5)\ (\langle n_E\rangle_T + 1), \qquad (1)$$

where $E^2 = \Delta^2 + W^2$, Δ and W are the asymmetry parameter and

tunneling frequency, ρ is the sample density and c is an average sound velocity. The phonon thermal occupation number $\langle n_E \rangle_T = (\exp(E/kT) - 1)^{-1}$. The f-parameter is related to the TLS_{ext} deformation potential [3, 5].

For the case where the anti-hole is significantly shifted away from the zero-phonon lines (ZPL) which are burned, the tunnel splitting E may be replaced by Δ, i.e., $\Delta \gg W$. It is generally assumed that f, W and Δ are not correlated and that an average value for f^2 in Eq. 1 can be used [5]. An approach for configurational averaging of Eq. 1 has been given [40, 41]. However, because the tunneling frequency W depends exponentially on the tunnel parameter λ, $W = \omega_0 \exp(-\lambda)$, and λ depends on several parameters subject to statistical fluctuations due to disorder, it is reasonable to assert that the distribution of relaxation rates (R) should derive mainly from the distribution function for W^2 [18, 40, 41]. Concerning the temperature dependence for R, one observes that it is weak when the distribution for Δ is centered at Δ_0 and $\Delta_0 \gg kT$ for the temperature range of interest, *vide infra*. The data presented in the next section for OX 720 are consistent with this inequality. Thus, we write

$$R = \Omega_0 \exp(-2\lambda) \qquad (2)$$

where $\Omega_0 = 3 \langle f^2\Delta \rangle \omega_0^2/16\pi\rho c^5\hbar^5$. It has been argued that $\Omega_0 \approx \omega_0$ and that $\Omega_0 \approx 10^{12}$ s^{-1} is a reasonable estimate [42]. Since this value has been utilized in earlier work [5, 9, 14, 29, 30, 40, 41] its use is maintained for the present simulations. Because $\lambda \geq 0$, $R_{max} = \Omega_0$.

Define f(R) as the normalized distribution function for the TLS_{ext} relaxation rate so that with

$$D(t) = \int_0^{\Omega_0} dR\ f(R)\ \exp(-P\sigma\phi(R)t), \qquad (3)$$

1 - D(t) is the fractional ZPH depth following a burn for time t with a photon flux P. Here σ is the peak absorption cross-section for the ZPL and $\phi(R) = R/(R+k)$ is the NPHB quantum yield for a probe excited state lifetime of k^{-1} (a few nanoseconds for laser dyes). Equation (3) is valid for a burn laser with a frequency width much narrower than the homogeneous line width of the ZPL. A form for f(R) is obtainable from the distribution function for W^2 which, in turn, is derivable from the distribution function for λ.

Elschner and Bässler [13, 15], Jankowiak and Small [18] and Jankowiak *et al.* [9, 12, 30] have argued that a Gaussian distribution function for λ is physically reasonable,

$$g(\lambda) = N_\lambda \exp\left[-(\lambda-\lambda_0)^2/2\sigma_2^2\right], \qquad (4)$$

when $\lambda_0^2/2\sigma_2^2 \gg 1$ (so that $g(0) \approx 0$). It will be shown that for OX 720, $\lambda_0^2/2\sigma_2^2 > 30$. Thus, physically unreasonable negative values for λ may be admitted with no introduction of error; the normalization constant $N_\lambda = (\sigma_2\sqrt{2\pi})^{-1}$. At the same time, the upper limit of the integral in Eq. 3 may be extended from Ω_0 to $+\infty$. Using Eq. 4, Jankowiak *et al.* have shown that [14]

$$f(R) = \frac{N_\lambda}{2\,\Omega_0}\,\lambda_2\left(\frac{R}{\Omega_0}\right)^{-\alpha}\exp\left[-\gamma\left(\ln\frac{R}{\Omega_0}\right)^2\right], \qquad (5)$$

where $\alpha = 1 + \lambda_0/(2\sigma_2^2)$, $\gamma = (8\sigma_2^2)^{-1}$ and $\lambda_2 = \exp\left[-\lambda_0^2/2\sigma_2^2\right]$.

For the simulations presented it is convenient to employ a particular form for D(t) which is equivalent to Eq. 3. Starting with

$$D(t) = N_\lambda \int_{\infty}^{-\infty} d\lambda\, \exp\left[-\frac{(\lambda-\lambda_0)^2}{2\sigma_2^2}\right] \exp\left[-P\sigma\phi(\lambda)t\right], \qquad (6)$$

and defining $x = (\lambda-\lambda_0)/\sigma_2$, it is easy to show that

$$D(t) = \sqrt{\frac{1}{2\pi}} \int_{-\infty}^{\infty} dx\, \exp(-x^2/2)\, \exp\left[-\Sigma_0\xi(x)t\right], \qquad (7)$$

where $\Sigma_0 = P\sigma\Omega_0/k$ and $\xi(x) = \exp\left[-2(\lambda_0-\sigma_2 x)\right]$. In deriving this equation it was assumed that for the majority of the TLS_{ext},

$$\phi(R) = R/(R+k) \approx R/k \ll 1. \qquad (8)$$

This assumption, based on earlier studies which showed that the average NPHB quantum yields are low ($< 10^{-4}$ [14, 18]) is readily tested by the experimental data.

Equation 7 was utilized for the simulations of the hole growth curves presented below. (Bode's approximation was utilized for numerical integration, see Appendix B.) Equation 7 neglects the contribution to dispersive growth associated with the utilization of linearly polarized burn and read beams [43]. In Section V it is shown that the orientational averaging has a weak affect on the hole growth kinetics during the initial stages of burning (hole depth less than $\approx$ 50% of the saturated depth). Its primary effect is to alter slightly the value of λ_0. Also Eq. 7 does not account for hole filling processes which occur during the course of the burn, cf. Section V for discussion.

IV. RESULTS

A. General Features of the Oxazine 720 Hole Spectrum

Zero-phonon hole (ZPH) growth kinetics for OX 720 in glycerol and PVOH have been studied with very low burn intensities ($5 \leq I_B \leq 1000$ nW/cm^2) which indicates that the NPHB quantum yields are unusually high. In the study of hole growth kinetics it is important to use I_B values which are sufficiently low to insure that the ZPH peak intensity being probed is not perturbed by phonon-sideband holes (PSBH) during the course of the burn. The problems presented by utilizing I_B values (and burn times) that are too high are apparent from Fig. 4 for which I_B = 1 mW/cm^2 (t_B = 5 min). Very similar ΔA spectra have been obtained for OX 720 in PVOH. The figure shows that the sharp ZPH at ω_B = 15803 cm^{-1} is superimposed on the high energy side of the broad pseudo-PSBH at ω_B − 27 cm^{-1} (mean phonon frequency ω_m = 27 cm^{-1}). In fact the ZPH saturates (reaches maximum peak intensity) for burn fluences several orders of magnitude lower than that used to obtain Fig. 4. Therefore, an essential part of the protocol for measurement of the hole growth curves included scanning of the ZPH following termination of the burn in order to determine that the ZPH in the ΔA spectrum emerged from a <u>flat</u> baseline.

Figure 4: Hole spectrum of Oxazine 720 in glycerol. Conditions: I_B = 1 mW/cm^2, t_B = 5 sec, ω_B = 15803 cm^{-1} and $T_B = T_R$ = 1.6 K. A number of pseudo-vibronic holes appear at $\omega < \omega_B$, e.g., at 302 cm^{-1} and 594 cm^{-1}. The real vibronic hole corresponding to the latter is at ω_B + 592 cm^{-1}. The pseudo-phonon sideband hole is indicated at ω_B − 27 cm^{-1}. Insert shows enlargement of the ZPH region; the real PSBH is apparent at ω_B + 27 cm^{-1}

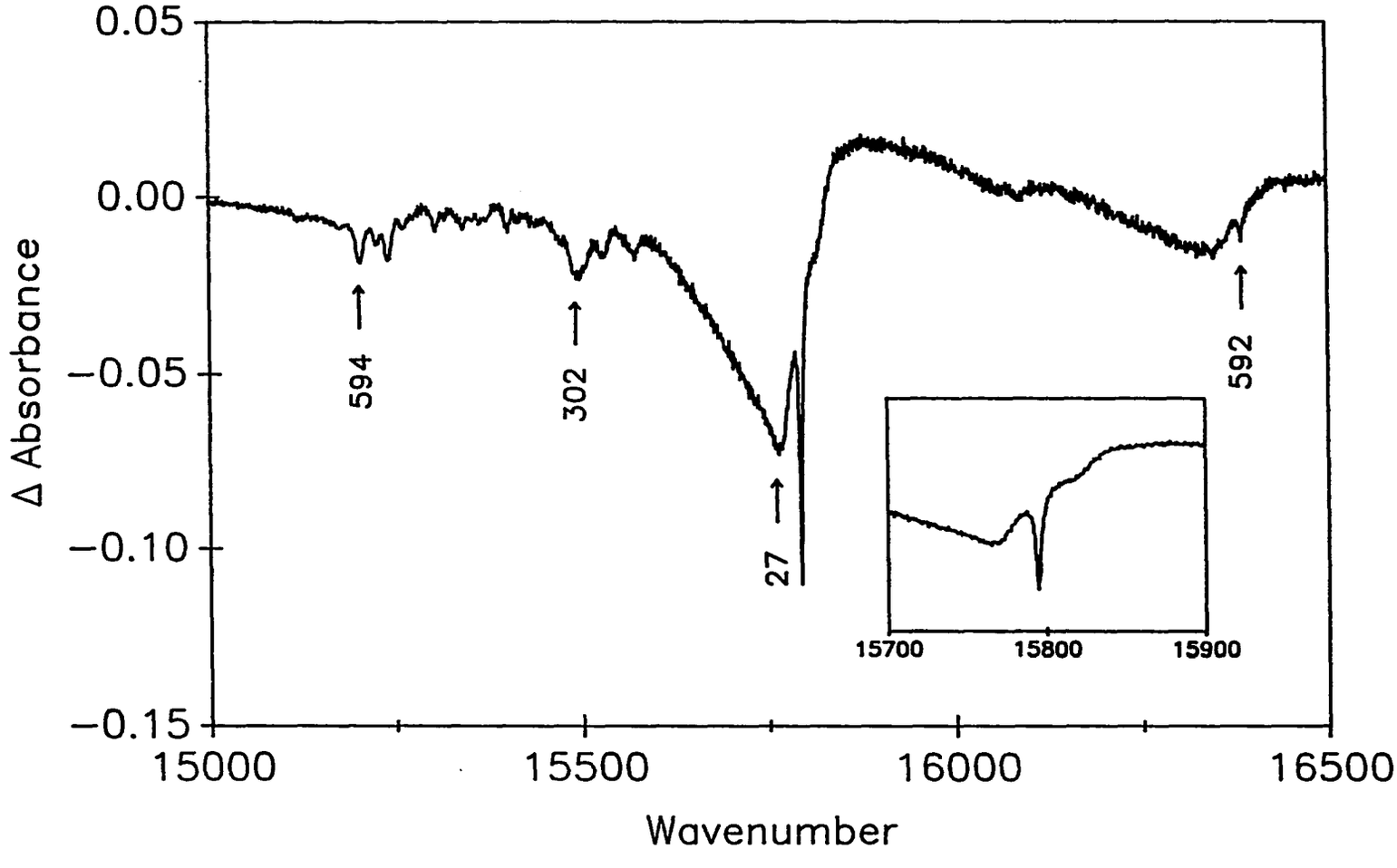
0.05
0.00
−0.05
−0.10
−0.15
Δ Absorbance
15000
15500
16000
16500
Wavenumber
594
302
27
592
15700
15800
15900

Figure 4 also illustrates that the mechanism for hole growth is nonphotochemical. As is the case for other systems involving $\pi\pi^*$ optical transitions [24, 27] the anti-hole lies predominantly to the blue of the pseudo-PSBH and ZPH (ω_B). In Fig. 4 the anti-hole has an "apparent" [44] maximum at ω_B + 60 cm^{-1} and tails several hundred cm^{-1} to higher energy. Interference with the anti-hole from real vibronic satellite holes at ω_B + 302 cm^{-1} and ω_B + 592 cm^{-1} is apparent. Pseudo-vibronic satellite holes which occur to lower energy of ω_B are also evident, cf. caption.

The inset of Fig. 4 shows more clearly the existence of the real-PSBH at ω_B + $\approx$25 cm^{-1}. Its interference with the anti-hole means that the actual anti-hole maximum is several cm^{-1} to the red of the apparent maximum.

B. Role of Linear Electron-Phonon Coupling

Although in the study of the ZPH growth kinetics the interference due to the PSBH can be avoided, *vide supra*, the linear electron-phonon coupling must still be taken into account in the theoretical analysis of the ZPH kinetics. This is because the optical density at ω_B is apportioned between the ZPL and phonon sideband transitions. Hayes and Small [45] and Hayes *et al.* [46] have developed a reliable theory for the overall hole profile (ZPH plus PSBH) which is valid for arbitrarily strong coupling. Recently, the theory

has been applied to several systems [47-49]. Although the theory can be incorporated into the formalism for hole growth described in the previous section, the present work does not do so (the computation time would be significantly increased). Instead, a result of the theory outlined in Refs. [45-49] will be utilized. This result states that for ω_B near the mean frequency of the distribution for ZPL excitation frequencies, the ratio of the integrated intensity of the ZPH to the total intensity (ZPH plus PSBH) is $\approx \exp(-2S)$ in the short burn time limit. Figures 5 and 6 present the results of a burn time dependent study for OX 720 in PVOH and glycerol, respectively. As expected [46, 50] the above ratio decreases with increasing burn time; only the pseudo-PSBH at $\omega_B - 27$ cm^{-1} is discernible in the figures. A plot of the intensity ratios versus burn time is shown in Fig. 7 for both amor-phous hosts. Upon extrapolation of both curves, an estimate for S of 0.3 - 0.5 can be determined. Unfortunately, this procedure does not lend itself to a precise determination for S since the pseudo-PSBH becomes difficult to measure in the short burn time limit. If, for example, S = 0.45, the Franck-Condon factor, exp(-S), for the ZPL is 0.65. The implication for hole burning is that the maximum (saturated) fractional ZPH depth should be $\approx$ 0.65. That is, $\approx$ 35% of the optical density at ω_B would be due to phonon-sideband absorption.

Figure 5: Burn time dependent hole spectra for Oxazine 720 in PVOH. Conditions: $T_B = T_R = 1.6$ K, $I_B = 1$ mW/cm^2 and $\omega_B = 15385$ cm^{-1}. Only the pseudo-phonon sideband hole at $\omega_B - 27$ cm^{-1} is discernible. Burn times from top to bottom are 30, 60, 90, 270 and 570 sec

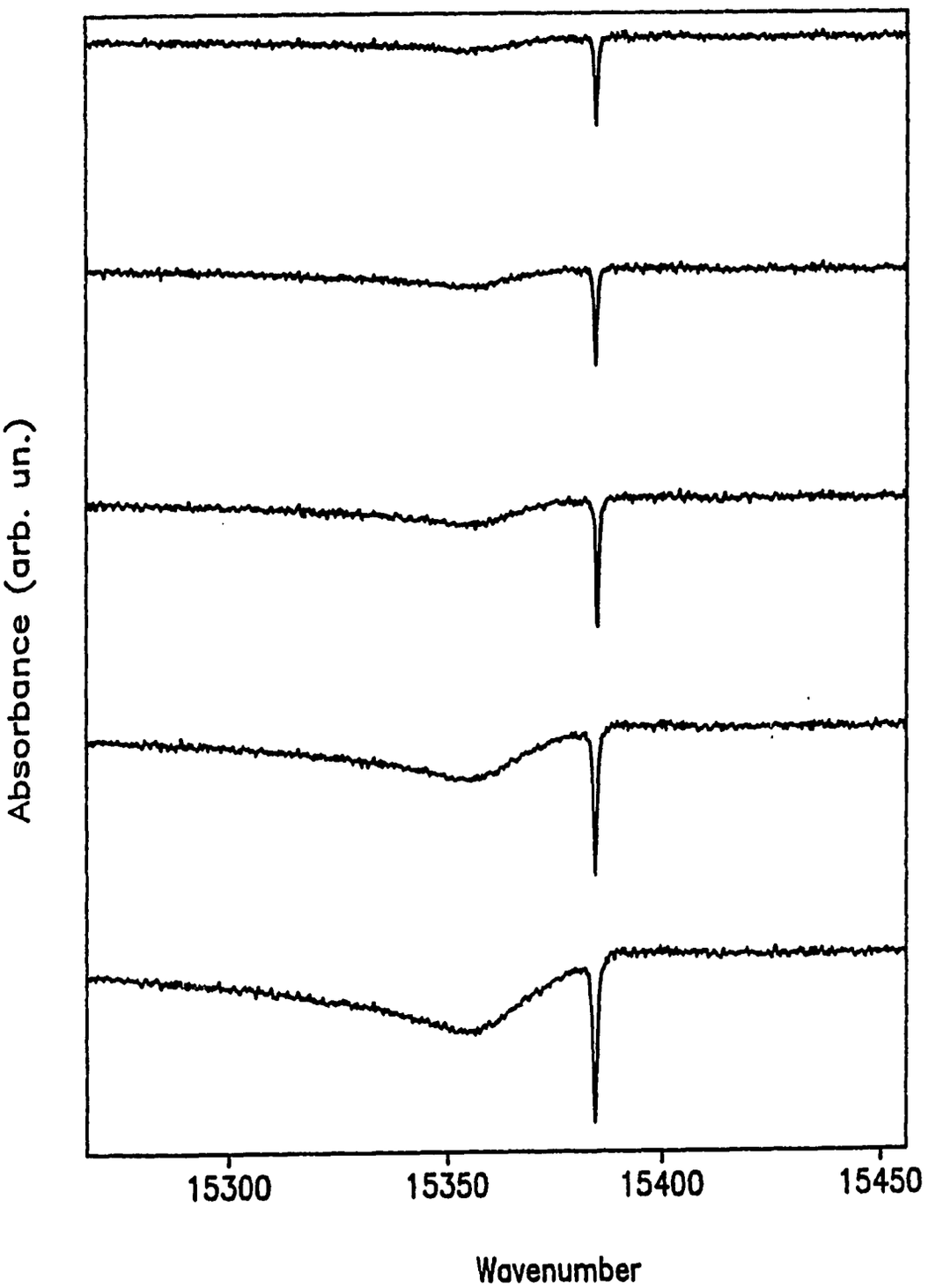
Absorbance (arb. un.)
15300
15350
15400
15450
Wavenumber

Figure 6: Burn time dependent hole spectra for Oxazine 720 in glycerol. Conditions and burn times are identical to those for Fig. 5

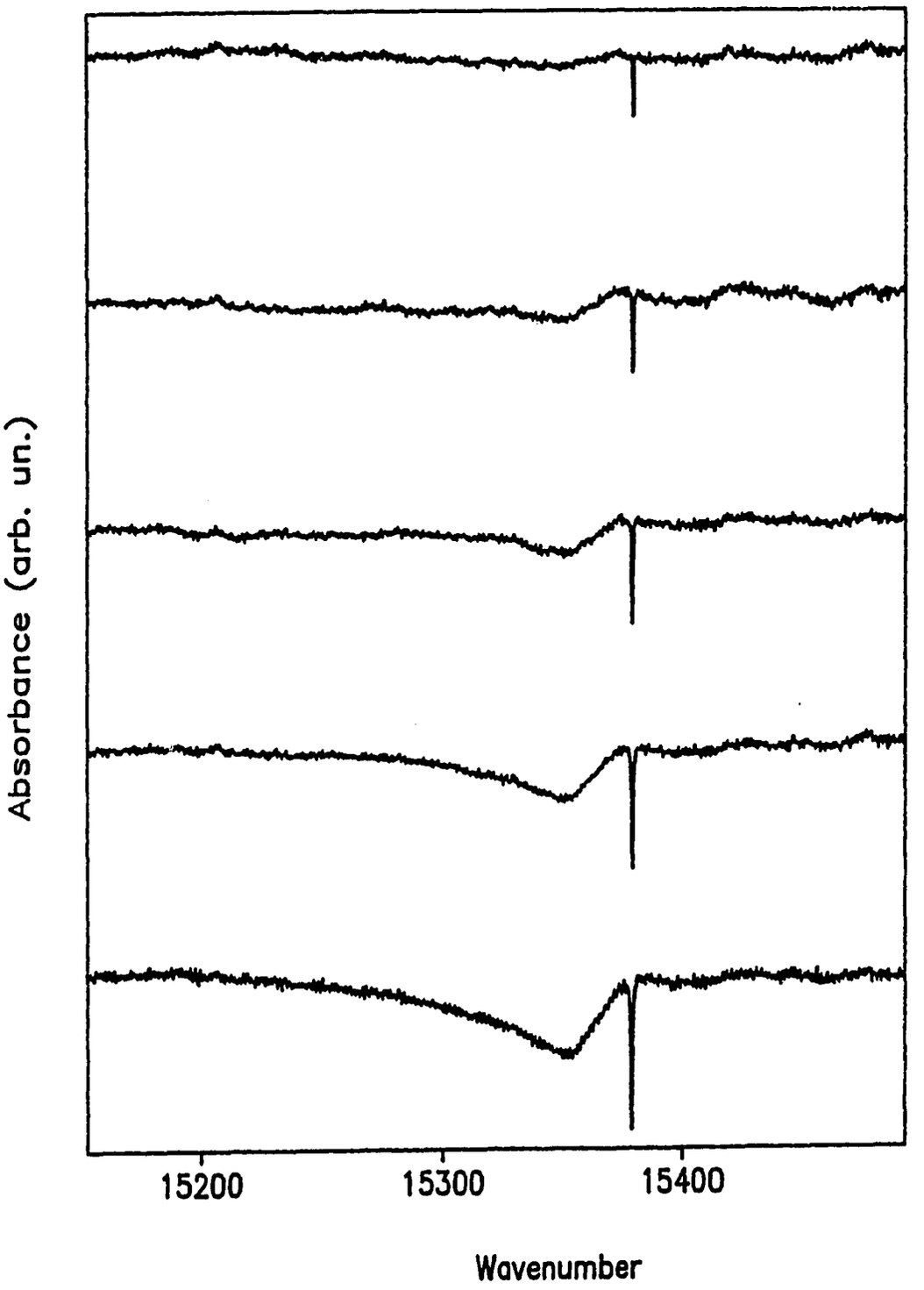
Absorbance (arb. un.)
15200
15300
15400
Wavenumber

Figure 7: Ratio of the integrated ZPH intensity to the total hole intensity, ZPH + PSBH, versus burn time for Oxazine 720 in glycerol and PVOH. Data are from Figs. 5 and 6. Note that the lines are meant only as a guide for the reader

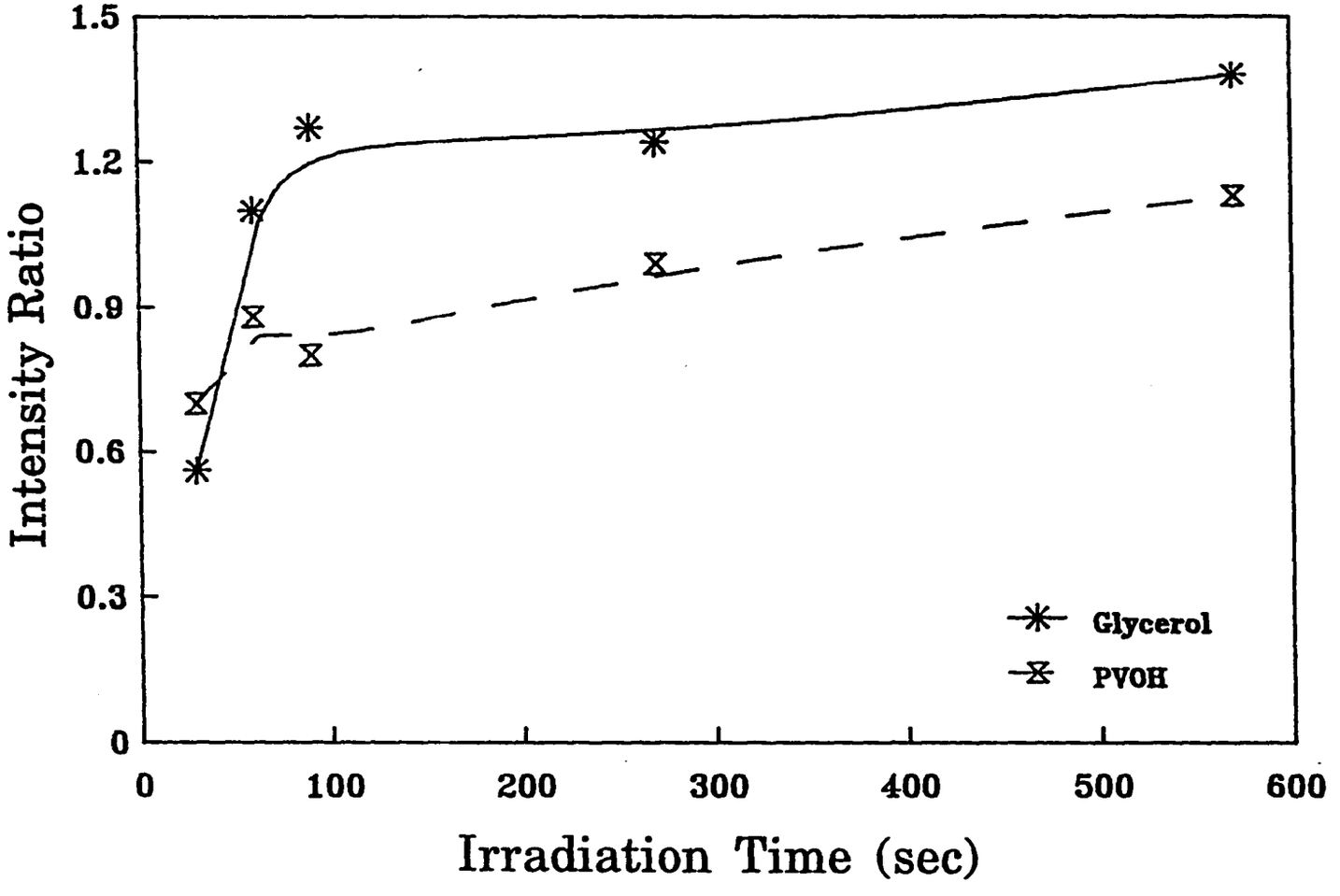
1.5
1.2
0.9
0.6
0.3
0
Intensity Ratio
0
100
200
300
400
500
600
Irradiation Time (sec)
Glycerol
PVOH

The above estimated range for S is consistent with the ZPL hole growth curves shown in Fig. 8 for OX 720 in PVOH and glycerol. A value of S = 0.45 was used in the simulations for both systems. Small variations (± 10%) about this value have only a weak effect on the values of λ_0 and σ_2.

In fitting Eq. 7 to the experimental hole growth curves a simple obvious renormalization was employed to take into account the off-set due to the fact that with S = 0.45 the maximum fractional hole depth is 0.65.

C. Dispersive Hole Growth Kinetics

1. Oxazine 720 in protonated glycerol glass

Hole growth curves are shown in Fig. 9 for I_B = 3.8, 38 and 380 nW/cm^2 and T_B = 1.6 K. The curves (solid) are plotted on a log t scale with the vertical scale giving the relative hole depth (e.g., 0.4 corresponds to a 60% OD change). The simulations from Eq. 7, which are indicated by symbols, were obtained with λ_0 = 7.7, σ_2 = 0.8 and S = 0.45. The values for k and σ (absorption cross-section) are given in the caption and were determined as discussed in the Experimental section. The value employed for Ω_0, Eq. 2, is 10^{12} s^{-1}, cf. Theory section. Considering that the burn intensity varies over two decades and the fluence over about five decades, the theoretical fits are viewed as good. It

Figure 8: Hole growth curves for Oxazine 720 in glycerol glass (top curve) and PVOH (bottom curve). I_B = 380 nW/cm^2 and 3.8 μW/cm^2 for glycerol and PVOH respectively; ω_B = 15408 cm^{-1} and T_B = 1.6 K. The maximum (saturated) fractional ZPH depth (in both cases) is consistent with the estimated range for S for Oxazine 720 in glycerol and also for Oxazine 720 in PVOH, see Fig 7. See text for details. Inset: structure of Oxazine 720

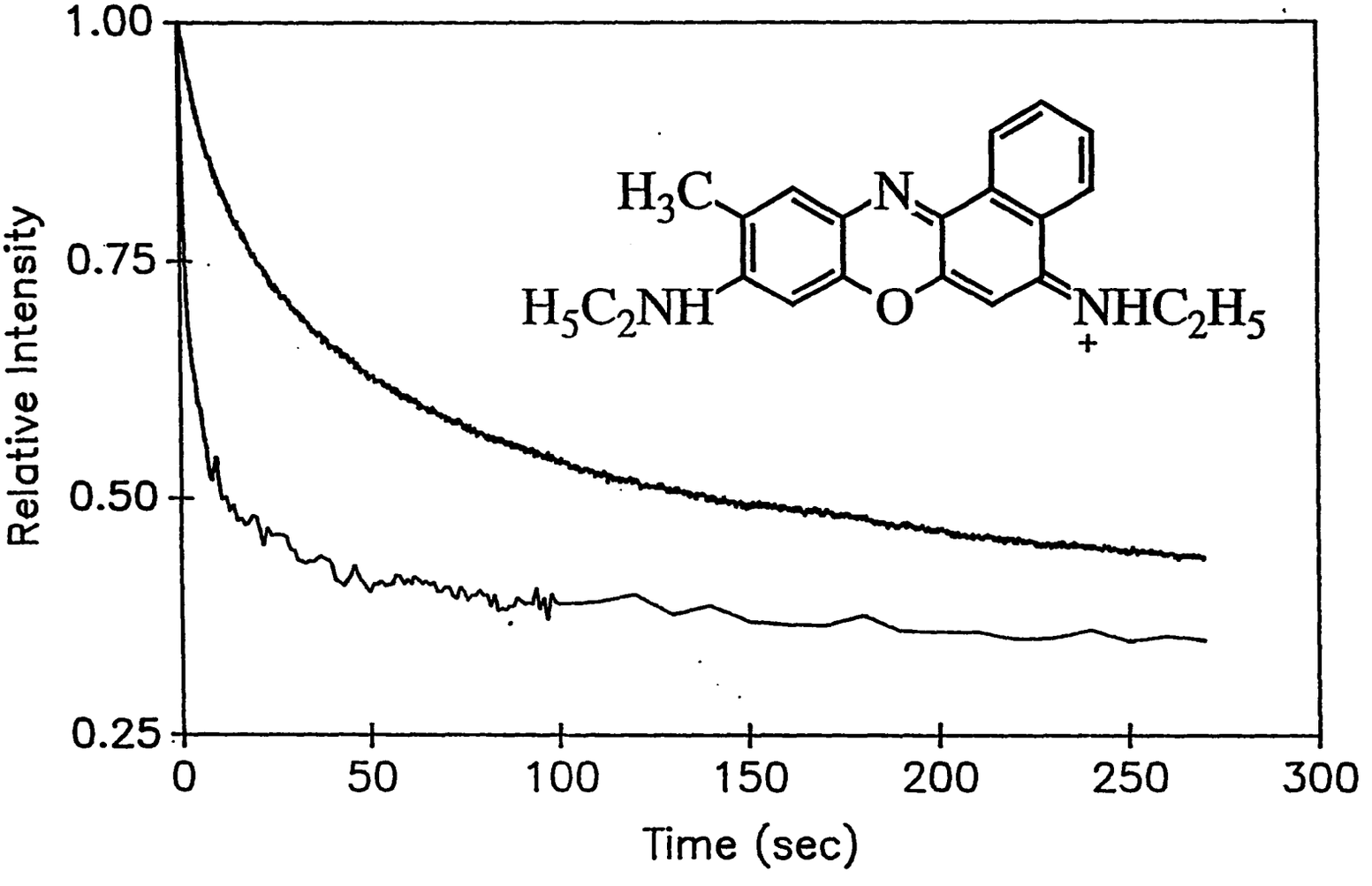
1.00
0.75
0.50
0.25
Relative Intensity
0
50
100
150
200
250
300
Time (sec)
H_3C
N
H_5C_2NH
O
NHC_2H_5
+

Figure 9: Zero-phonon hole growth for Oxazine 720 in a glycerol glass plotted on a log t_B scale. Burn intensities given in the figure; T_B = 1.6 K and ω_B = 15408 cm^{-1}. Solid curves are experimental while symbols are theoretical fits obtained with σ = 40 x 10^{-12} cm^2, Ω_0 = 10^{12} s^{-1}, S = 0.45 and k = 3.7 x 10^8 s^{-1}. Fits shown are for λ_0 = 7.7 and σ_2 = 0.8

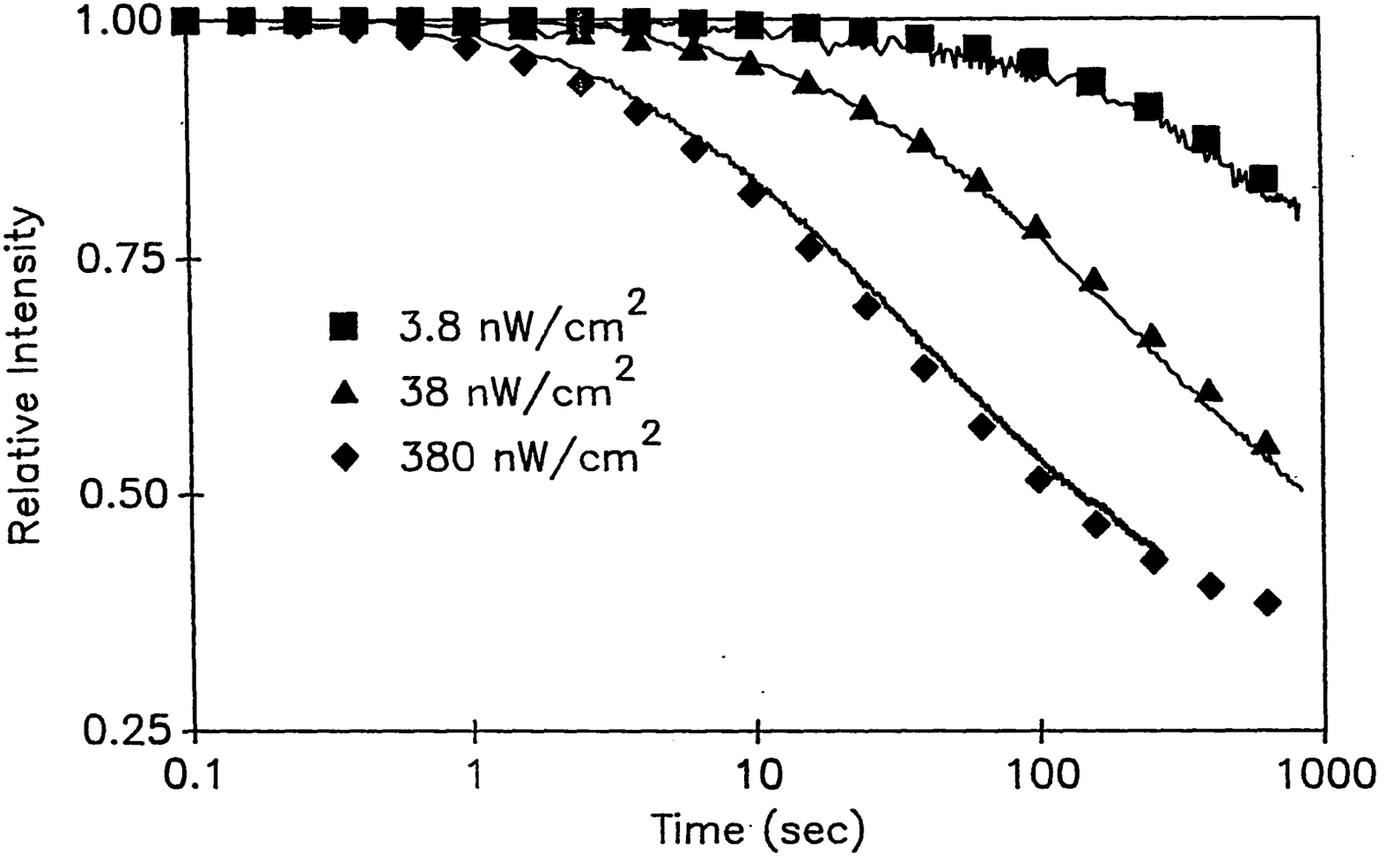
1.00
0.75
0.50
0.25
Relative Intensity
3.8 nW/cm2
38 nW/cm2
380 nW/cm2
0.1
1
10
100
1000
Time (sec)

is instructive to compare the 380 nw/cm^2 curve of Fig. 9 with the corresponding curve in Fig. 8 where hole growth is plotted on a linear burn time scale. Agreement between experiment and theory can be more critically assessed from log t plots.

Figure 10 shows the single frequency scans of the ZPH for the two lowest burn intensities presented in Fig. 9. The sample OD was 0.6 at the burn wavelength for both samples. The upper trace shows a ΔOD of 0.12 corresponding to a 20% hole while the lower trace represents a ΔOD of 0.3 which is a 50% hole. Note that the spectra have been offset for clarity.

Several features should be noted in Fig. 10. First, the baseline in both spectra is flat which indicates that there is no interference between the ZPH and phonon-sideband holes. As stated previously, this is an essential requirement for the study of hole growth kinetics. Second, the FWHM of the smaller hole is $\sim$ 0.8 GHz while the larger hole is $\sim$ 1.1 GHz. The observation that the FWHM does not change significantly, 38%, while, at the same time, the hole depth does increase significantly, 150%, indicates that the hole has not yet saturated. Data will be presented which demonstration the effect of hole saturation. (Note: A trace for the highest intensity burn is not presented due to laser instabilities subsequent to hole growth analysis.)

Figure 10: Zero-phonon hole spectra corresponding to the 3.8 and 38 nW/cm^2 hole growth curves of Fig. 9. The upper trace (lower I_B) represents a ΔOD of 0.12 corresponding to a 20% hole while the lower trace exhibits a ΔOD of 0.3 corresponding to a 50% hole. The spectra have been offset for clarity

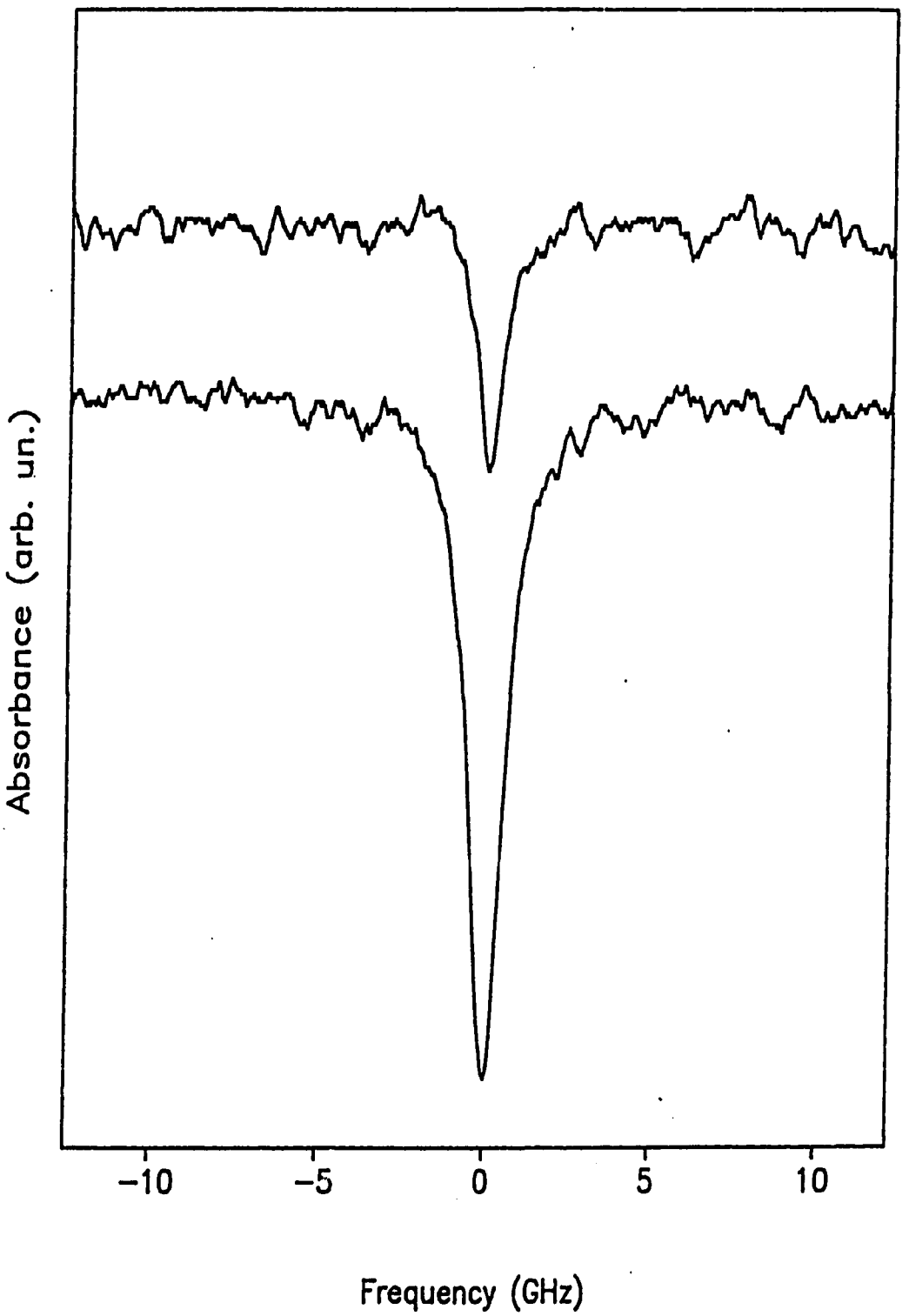
Absorbance (arb. un.)
−10
−5
0
5
10
Frequency (GHz)

The data of Fig. 9 were obtained during a single run in which there was no sample temperature cycling or optical realignment. Data from other runs were found to be in satisfactory agreement. As an example, Fig. 11 shows growth curves for I_B = 10 and 100 nW/cm^2 along with the simulations obtained with λ_0 = 7.9, σ_2 = 0.8 and S = 0.45. Figure 12 presents the ZPH spectra for the data of Fig. 11. The increased noise level observed results from a lower sample OD than that of Fig. 10, sample OD = 0.3. The important features of Fig. 12 are the flat baseline of both spectra and the small increase in the FWHM for the higher intensity burn. The simulated curves in Fig. 13 are useful for a consideration of the discrepancy between theory and experiment in Fig. 11. The former figure shows the dependence of hole growth on σ_2 with curves for σ_2 = 0.0, 0.6, 0.8 and 1.0 (a, c, d and e) obtained with λ_0, S and I_B fixed at 7.8, 0.45 and 380 nW/cm^2 (the curve related to configurational averaging (b) will be considered in the Discussion section). For σ_2 = 0.0 the growth kinetics are non-dispersive (single exponential). Note than an increase in σ_2 causes a raising and lowering of the growth curve to the right and left of the isointensity hole point. This point occurs at 50% of the maximum hole depth. The effect of varying λ_0 with the other parameters held fixed can be understood with Eq. 7. The effect is one of simply shifting

Figure 11: Zero-phonon hole growth for Oxazine in a glycerol glass at 1.6 K. See Fig. 9 caption. Fits (symbols) are for $\lambda_0 = 7.9$ and $\sigma_2 = 0.8$

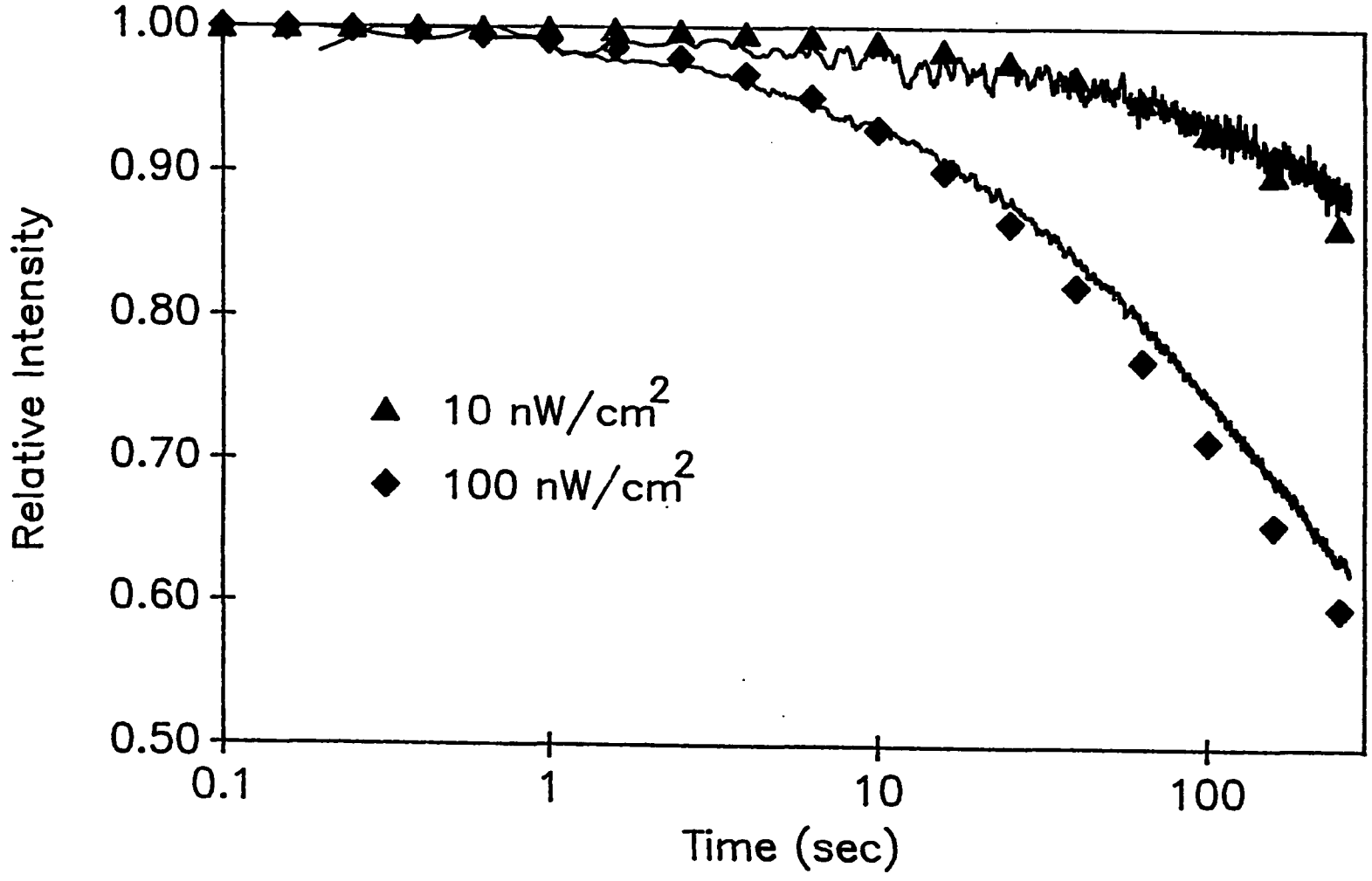
1.00
0.90
0.80
0.70
0.60
0.50
Relative Intensity
10 nW/cm2
100 nW/cm2
0.1
1
10
100
Time (sec)

Figure 12: Single frequency scans of the ZPH corresponding to the hole growth curves of Fig. 11. The upper curve has a ΔOD of 0.035 corresponding to a 12% hole while the lower trace represents a 38% hole, ΔOD = 0.11

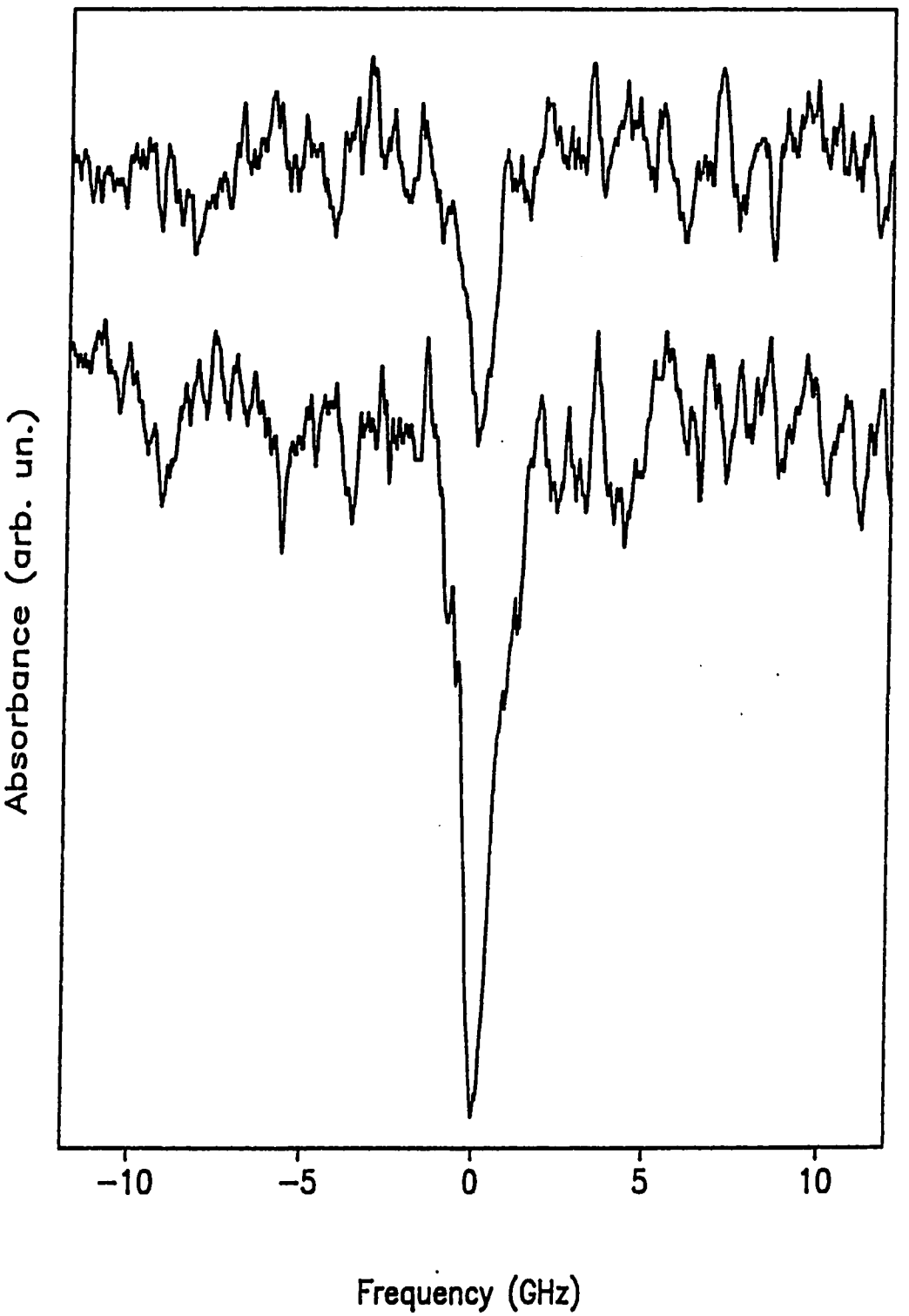
Absorbance (arb. un.)
−10
−5
0
5
10
Frequency (GHz)

Figure 13: Calculated dependence of zero-phonon hole growth on σ_2. Curves calculated with values for σ, Ω_0, S and k given in Fig. 9 caption, $\lambda_0 = 7.8$ and $I_B = 380$ nW/cm^2. Curves a, c, d and e are for $\sigma_2 = 0.0$ (no dispersion), 0.6, 0.8 and 1.0 with no orientational averaging. Curve b obtained with orientational averaging and $\lambda_0 = 7.5$ (see Discussion section)

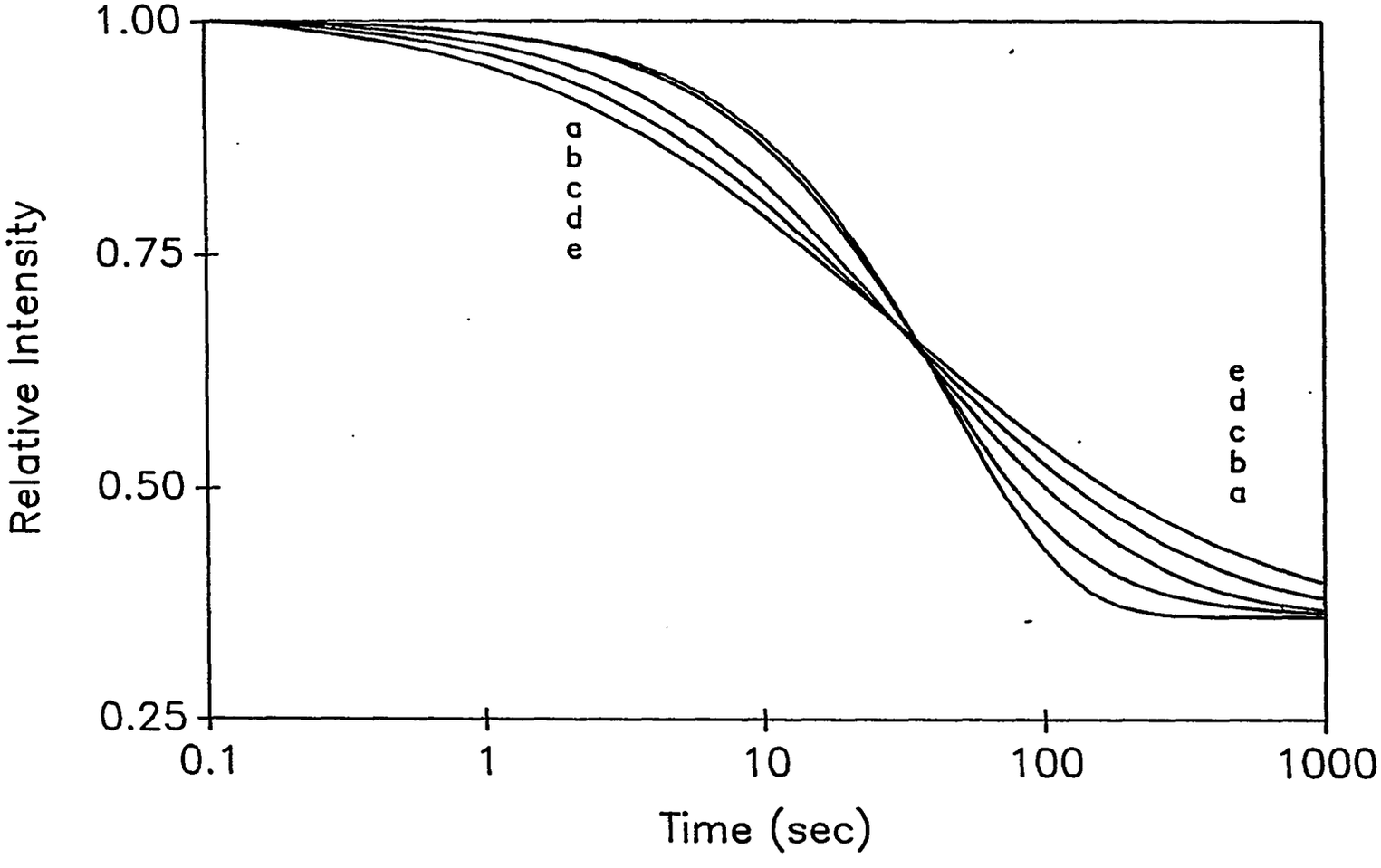
1.00
0.75
0.50
0.25
Relative Intensity
0.1
1
10
100
1000
Time (sec)
a
b
c
d
e
e
d
c
b
a

the growth curves to the right or left on the log t scale. For example, increasing λ_0 by unity shifts the growth curve to the right by 0.9 on a log t scale. With this in mind and the σ_2 dependence shown in Fig. 13 one might estimate that by increasing σ_2 from 0.8 to ~ 1.0, the fits in Fig. 11 would be significantly improved and this is actually the case (simulations not shown).

The effect of varying the photon flux P (or equivalently the absorption cross-section σ) on hole growth is also apparent from Eq. 7. For example, if the measured flux yields a value for λ_0 of λ_0' but the measurement is in error by 60% (on the high side), the correct value for λ_0 would be $\lambda_0' - (\ln 0.6)/2 = \lambda_0' + 0.25$. As stated previously, the uncertainty in the measurement of the relative burn intensities during a given run is smaller, < 10%.

Figures 14 and 15 present data from another set of experiments for OX 720 in a glycerol host. For these curves, I_B = 22, 220 and 3000 nW/cm^2 and T_B = 1.6 K. The sample OD was 0.3. Simulations using Eq. 7 are presented and were determined using values of λ_0 = 7.8, σ_2 = 1.1 and S = 0.6. Other parameters are given in the caption. The value of S used for these simulations is different from those used previously. The ZPH spectra corresponding to the hole growth curves of Fig. 14 are presented in Fig. 15. ΔOD

Figure 14: Zero-phonon hole growth curves for Oxazine 720 in glycerol. For these data theoretical fits were obtained with $\lambda_0 = 7.8$ and $\sigma_2 = 1.1$. In addition, the following constant values were used; $\sigma = 40 \times 10^{-12}$ cm^2, $\Omega_0 = 10^{12}$ s^{-1}, $k = 3.7 \times 10^8$ s^{-1} and $S = 0.6$. See text for a discussion of the change in the value for S

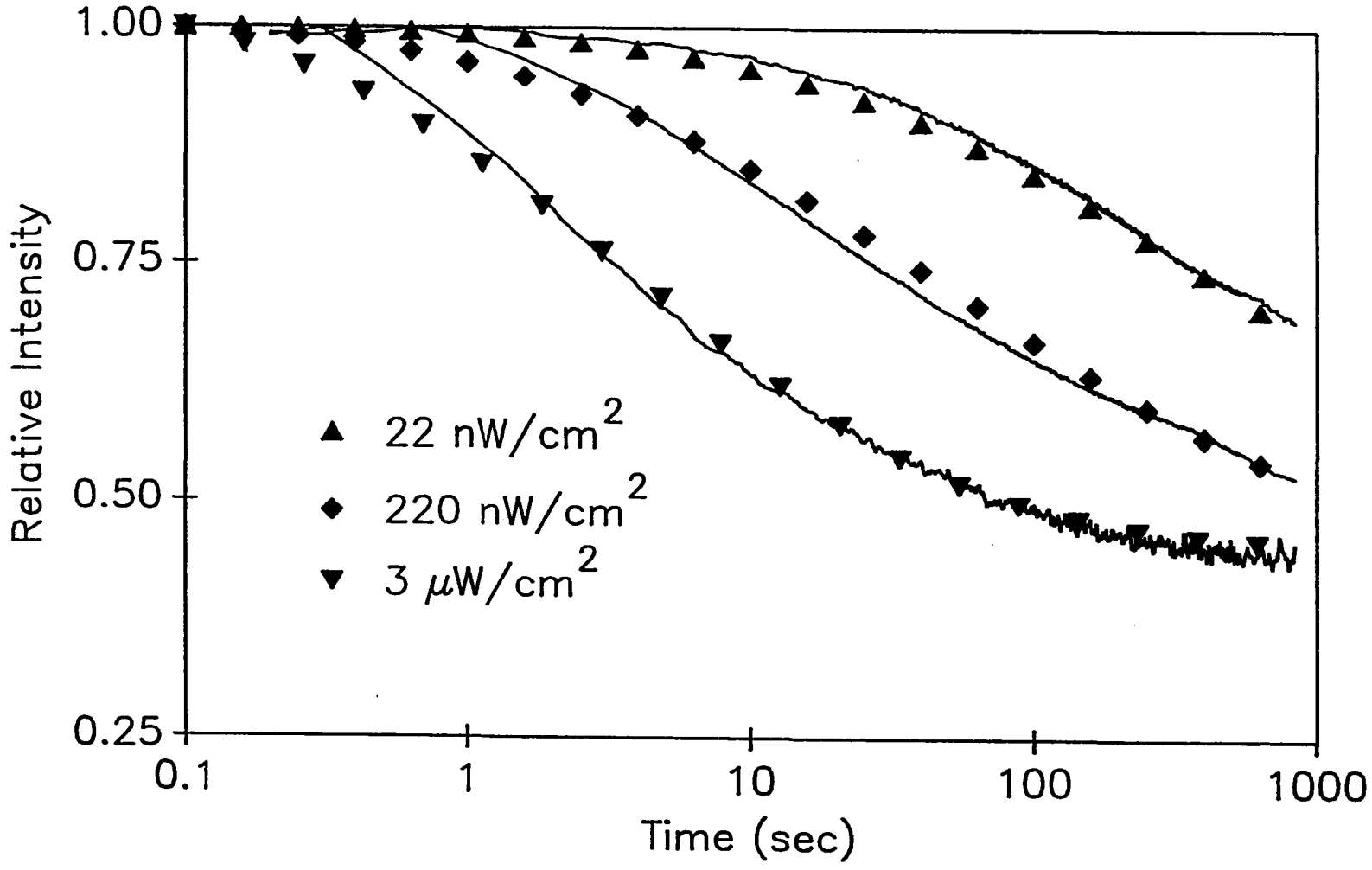
1.00
0.75
0.50
0.25
Relative Intensity
22 nW/cm2
220 nW/cm2
3 μW/cm2
0.1
1
10
100
1000
Time (sec)

values are listed in the caption. As indicated in the caption of Fig. 15, the saturated depth of the highest intensity hole is 55% which is consistent with a value of S = 0.6 as discussed earlier. The cause for a new value of S is uncertain but the variation is within the uncertainty for these experiments.

During this set of experiments, the formation of a glass was more difficult than at other times during the course of these experiments. Several modifications to the sample preparation were attempted to eliminate these problems including distillation and drying of the solvent and variation of the cooling rate. None of these modifications improved glass formation nor did the modifications affect the saturation depth. Note that the data of Fig. 14 are taken from several weeks of experimentation and that, for all experiments, a consistent saturation point was observed.

It is important to note that the baseline for all three holes of Fig. 15 is flat as required for these studies. Comparison of the holes corresponding to the lowest burn intensities shows that these holes are not saturated, the hole width increases only slightly while the hole depth increases significantly. But, upon comparing the two holes corresponding to the highest burn intensities, it is observed that the FWHM for the highest burn intensity hole

Figure 15: Single frequency spectral scans for the holes corresponding to the hole growth curves of Fig. 14. The ΔOD values are 0.09, 0.15 and 0.165 from top to bottom. These correspond to 30, 50 and 55% holes. The measured hole widths are 1, 1 and 4.2 GHz, respectively

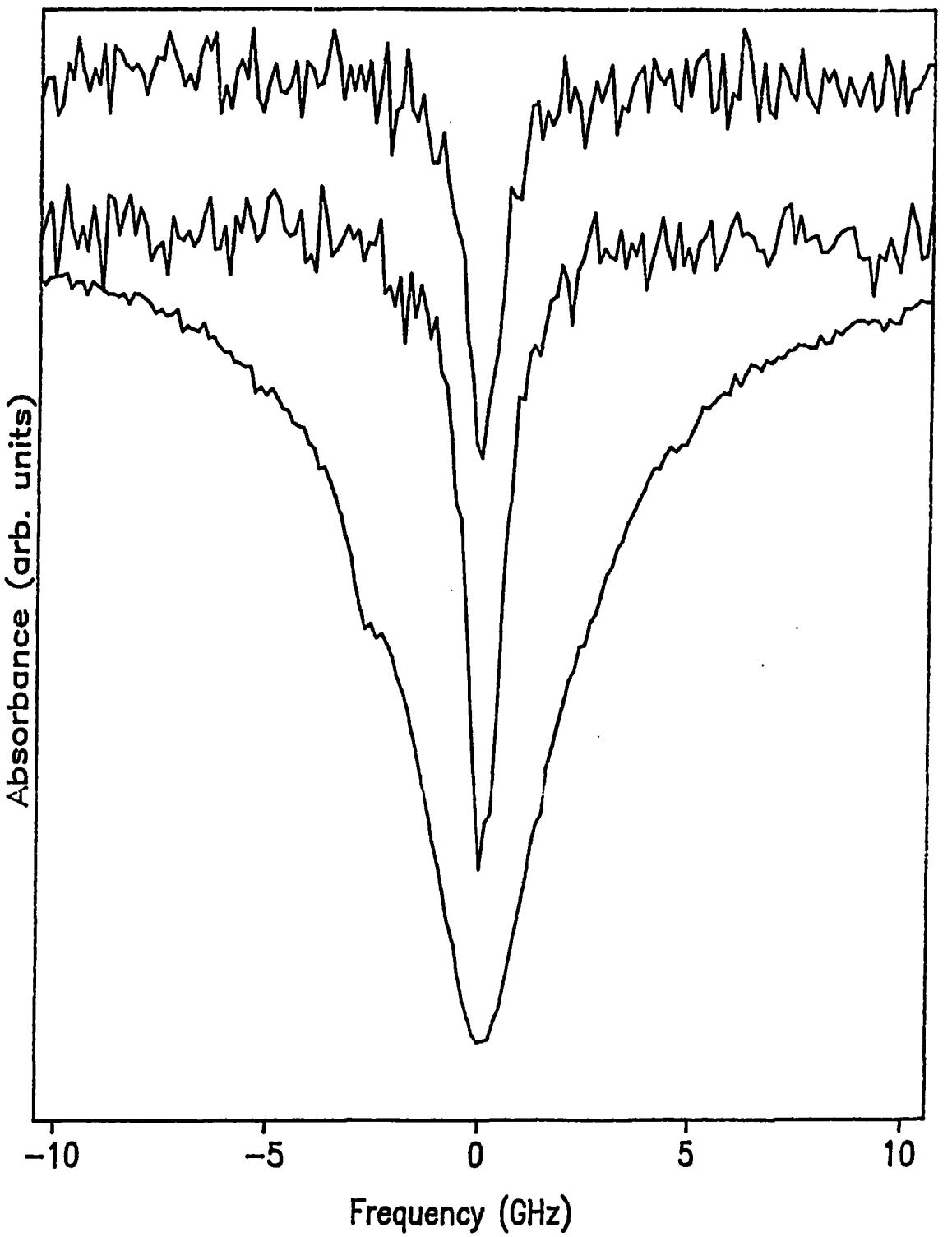
Absorbance (arb. units)
−10
−5
0
5
10
Frequency (GHz)

has increased dramatically, ~ 300%. At the same time, the depth of this hole has increased only slightly, ~ 20%. The combination of these two effects demonstrates that the hole has saturated and that additional non-resonant ZPL are being burned via absorption through the tails of the homogeneous absorption lines which overlap the resonant ZPL.

Saturation is also evident from the hole growth kinetic curve of Fig. 14. Note how quickly the 3 $\mu W/cm^2$ burn intensity hole is produced relative to the lower burn intensities. In addition, the data of Fig. 14 show that the hole depth is no longer increasing. Eq. 7 was derived with the assumption that the irradiation laser line width is less than the homogeneous line width of a single isochromat. The ZPH spectra of Fig. 15 clearly show that additional isochromats may be burned after all sites resonant with the burn frequency have been burned. In spite of these interferences, Eq. 7 is clearly very good at simulating the kinetics of hole growth.

Note as well that the value of $\sigma_2 = 1.1$ is also slightly increased from the earlier results. This observation may also be related to the difficulties in glass formation but can not be explained using these data.

2. Oxazine 720 in polyvinyl alcohol

Hole growth curves for OX 720 in PVOH from two separate runs are given in Fig. 16 for burn intensities that vary over three decades. The simulated fits were obtained with $\lambda_0 = 7.6$, $\sigma_2 = 1.0$ and $S = 0.45$. Considering that the dynamic range of the experiments is over five decades of burn fluence, the agreement with experiment is good. The above values for λ_0 and σ_2 in PVOH are similar to those for glycerol.

3. Effect of host deuteration

For hydrogen bonding glasses such as alcohols, the important observation has been that while the pure dephasing of the optical transition does not depend on deuteration of the hydroxyl proton, the NPHB efficiency is significantly reduced [37, 51]. The most reasonable interpretation is that the more rapid dephasing is due to tunneling of spatially extended TLS_{int} associated with hydrogen bonded networks and that hole burning is due to TLS_{ext} whose tunneling coordinate involves significant amplitude of motion for the hydroxyl proton. Delocalized coordinates of extended hydrogen bonded networks, which feature small amplitude atomic motions, have also been suggested as candidates for the TLS_{int} of amorphous water [52].

Figure 16: Zero-phonon hole growth curves for Oxazine 720 in polyvinyl alcohol film at 1.6 K. Fits (symbols) are for $\lambda_0 = 7.6$ and $\sigma_2 = 1.0$ with values for σ, Ω_0, S and k given in Fig. 9 caption. Deviation between theory and experiment for $I_B = 3.8\ \mu W/cm^2$ to $t_B < 1$ sec is a result of very high growth rate and limited time resolution

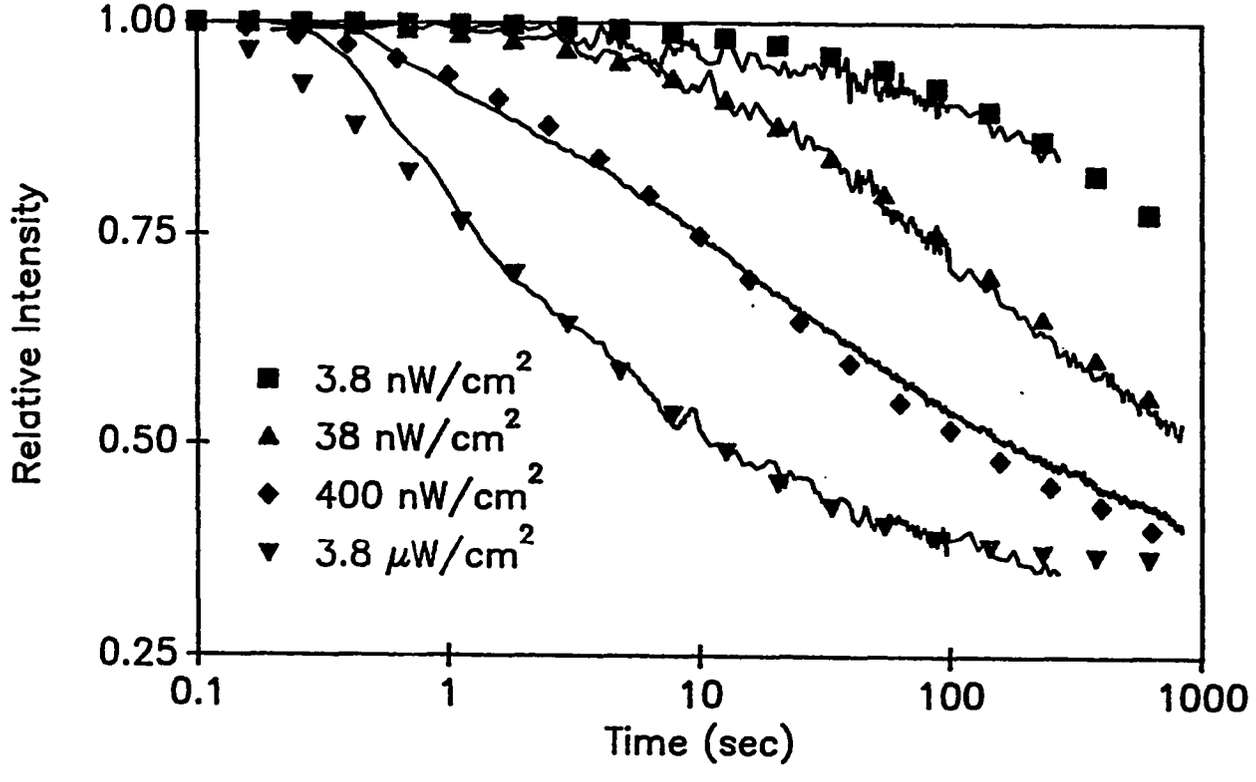
1.00
0.75
0.50
0.25
Relative Intensity
0.1
1
10
100
1000
Time (sec)
3.8 nW/cm^2
38 nW/cm^2
400 nW/cm^2
3.8 μW/cm^2

Figure 17 gives hole growth curves for OX 720 in PVOD (I_B = 400 nW/cm^2) and deuterated glycerol (I_B = 40 nW/cm^2). The simulations obtained with (λ_0, σ_2) = (9.4, 1.2) and (9.8, 1.0) for PVOD and deuterated glycerol, are in good agreement with the experimental curves. The λ_0 values, relative to those determined earlier for the protonated hosts, indicate that the TLS_{ext} coordinate is localized with significant amplitude of motion for the hydroxyl proton.

4. Effect of burn temperature

The dependence of the hole growth kinetics for OX 720 in glycerol on T_B has been studied over a limited range between 1.6 and 7.0 K in order to determine whether or not the hole burning efficiency or, more precisely, the distribution of hole burning efficiencies, depends on the burning temperature. Recent measurements on cresyl violet perchlorate in PVOH showed that, at best, the efficiency is weakly dependent on T_B between 1.6 and 15 K [53]. Figure 18 gives the OX 720 in glycerol growth curves for T_B = 1.6, 4.2 and 7.0 K. As with all other growth curves presented, it is the growth of the peak of the ZPH which is monitored. The fit to the 1.6 K curve (solid delta symbols) was obtained with λ_0 = 7.8, σ_2 = 0.8 and S = 0.45, values which were determined earlier. Since kT (T = 7 K) $\ll \omega_m$ = 27 cm^{-1} (the mean phonon frequency), the value for S(T) at 7 K and 4.2 K

Figure 17: Effect of host hydroxyl deuteration on hole growth kinetics for Oxazine 720 at 1.6 K. Burn intensities for PVOD and deuterated glycerol are 40 nW/cm^2 and 400 nW/cm^2; fits (symbols) obtained with (λ_0, σ_2) = (9.4, 1.2) and (9.8, 1.0), respectively. Values for σ, Ω_0, k and S are given in Fig. 9 caption

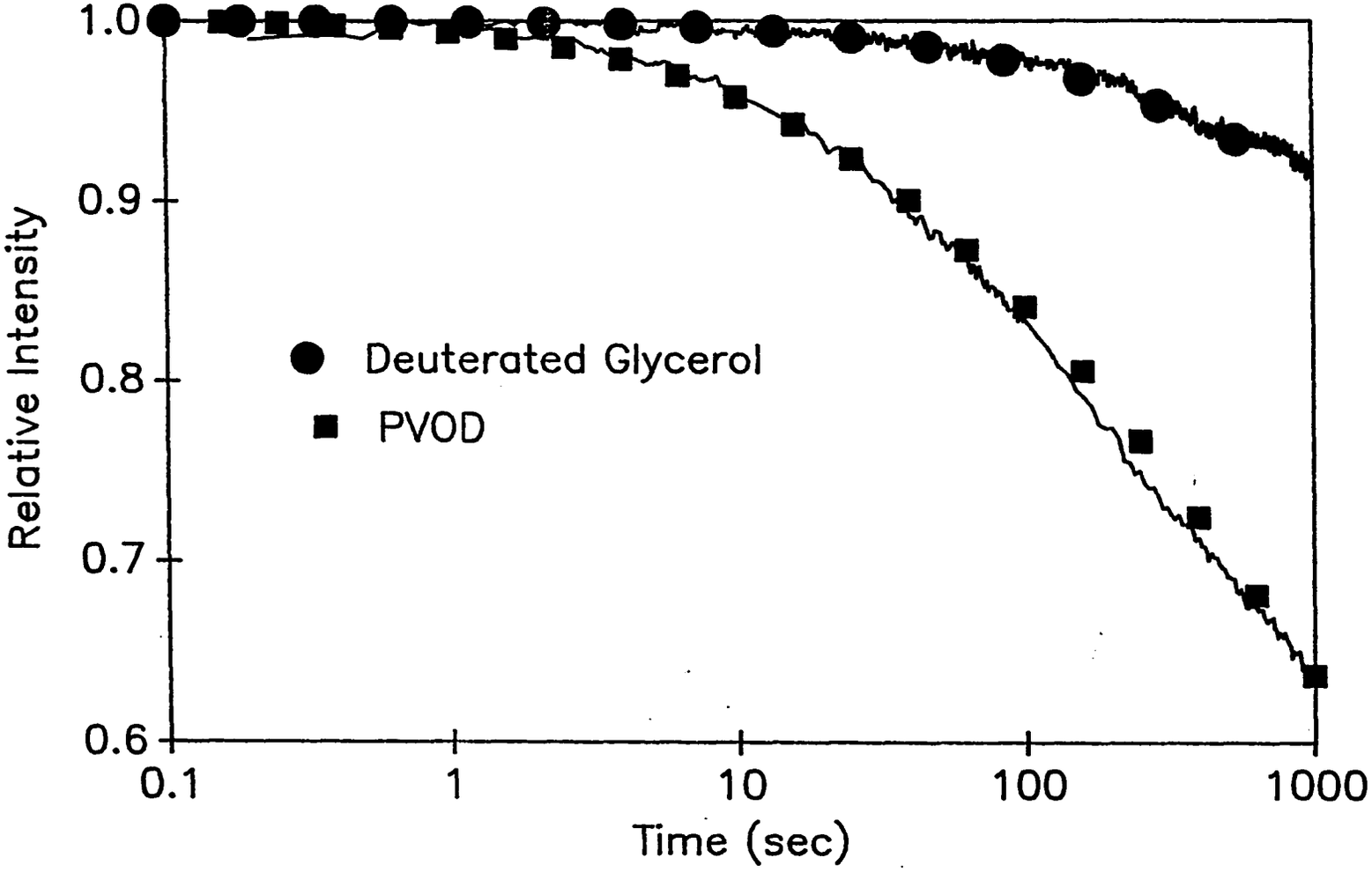
1.0
0.9
0.8
0.7
0.6
Relative Intensity
Deuterated Glycerol
PVOD
0.1
1
10
100
1000
Time (sec)

is unchanged from 0.45. Provided that λ_0 and σ_2 are independent of T_B, the temperature dependence of hole growth should be determined solely by the temperature dependence of the peak absorption cross-section, σ, i.e., the induced absorption rate. The cross-section is inversely proportional to Γ_H, the homogeneous line width of the ZPH. For a wide variety of molecules imbedded in amorphous hosts, $\Gamma_H \propto T^n$ with $n \sim 1.3$ in the low temperature regime [5, 54]. In Fig. 18 the simulations for the 4.2 and 7.0 K curves were obtained with $\lambda_0 = 7.8$ and $\sigma_2 = 0.8$ and σ values scaled from the 40×10^{-12} cm^2 value at 1.6 K by the $\Gamma_H \propto T^{1.3}$ power law. The good agreement with experiment indicates that the distribution of hole burning efficiencies is invariant in the above temperature range. It follows also that the growth curve for the integrated intensity of the ZPH versus burn fluence is independent of T_B.

5. Spontaneous hole filling

The kinetics of spontaneous hole filling (SPHF) for OX 720 in glycerol were also studied. SPHF is a dark ground state process which causes filling of the ZPH. Although the mechanism is not clearly understood, the effect upon hole growth kinetics is important to study. Due to the nature of the TLS model which describes the ground state TLS as having a different distribution of barrier heights and tunnel

Figure 18: Temperature dependence of zero-phonon hole growth for Oxazine 720 in a glycerol glass. The fits were obtained for $\lambda_0 = 7.8$, $\sigma_2 = 0.8$ and values Ω_0, k and S given in Fig. 9 caption. The value for $T_B = 1.6$ K is the same as in Fig. 9 while its value for $T_B = 4.2$ and 7.0 K were adjusted for temperature dependent dephasing (see text)

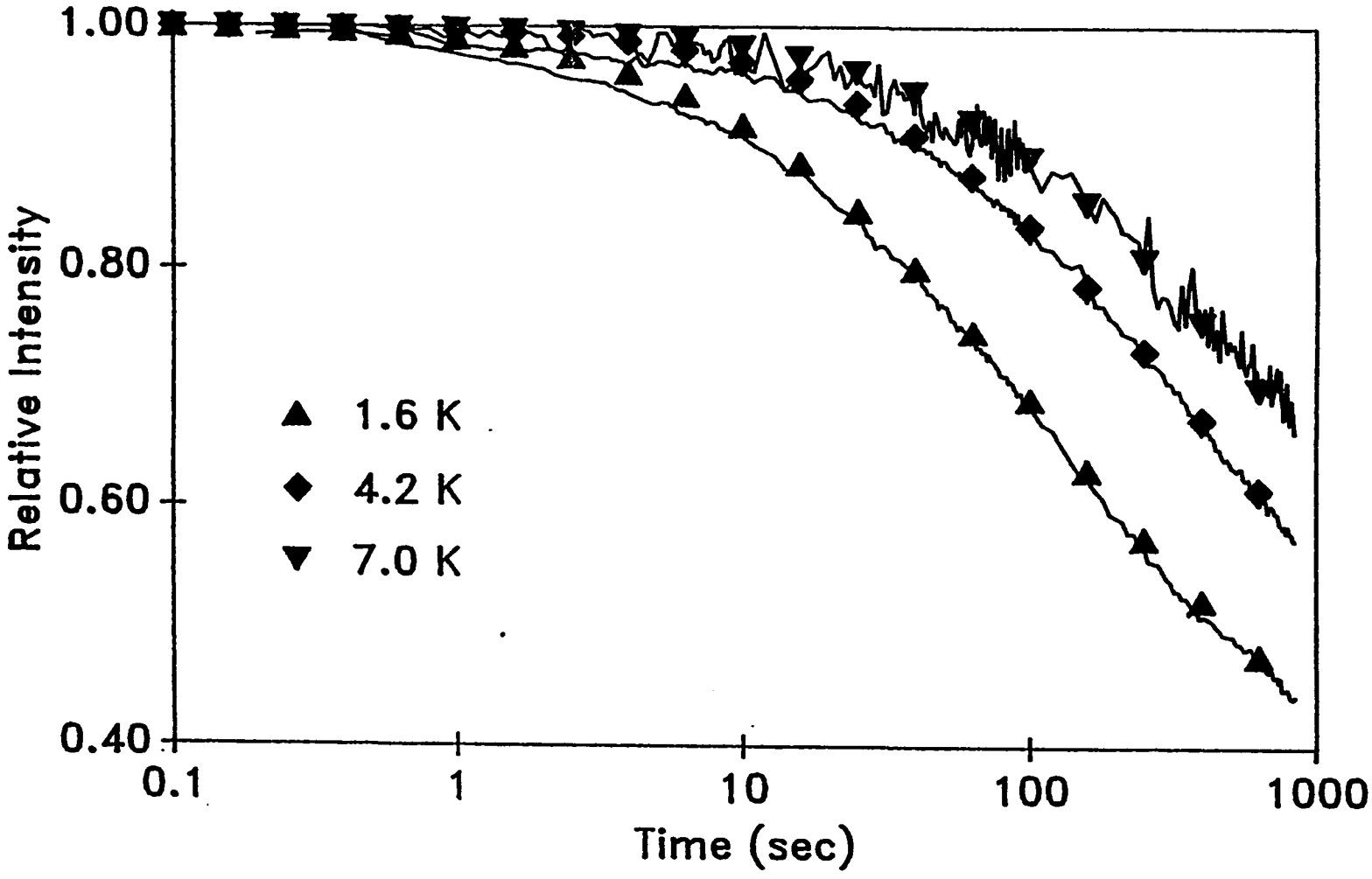
1.00
0.80
0.60
0.40
Relative Intensity
1.6 K
4.2 K
7.0 K
0.1
1
10
100
1000
Time (sec)

parameters, the distribution of relaxation times for SPHF is expected to be different from the distribution for hole growth.

For these studies, a hole was burned using a burn intensity chosen to produce a significant, $\Delta OD \sim 25\%$, yet unsaturated hole. The laser was then shuttered for a variable period of time. Subsequently, the laser was unshuttered and hole growth continued. By comparing the optical density at the end of the first irradiation period to the value at the onset of the second irradiation period, it was possible to determine the percentage of the hole which had filled during the dark period. The data points of Fig. 19 plot the ratio of the described optical densities versus the duration of the dark period. The solid line represents a simulation of the kinetics of hole filling using Eq. 7. For this analysis, $\Sigma_0 = \Omega_0$. The curve was obtained using $\lambda_0 = 18$ and $\sigma_2 = 1.5$. As demonstrated in the figure, the distribution function used to describe hole growth kinetics, Eq. 5, also describes the kinetics of spontaneous hole filling.

Figure 19: Spontaneous hole filling study for Oxazine 720 in glycerol. The y-axis plots $1 - \frac{\Delta OD_{after}}{\Delta OD_{before}}$, where after and before correspond to the variable dark period (see text), and the x-axis is the duration of the dark period. (A normalized intensity of 1.00 corresponds to a completely filled hole.) The fit (solid line) was obtained using Eq. 7 with $\lambda_0 = 18$, $\sigma_2 = 1.5$ and $\Sigma_0 = \Omega_0$

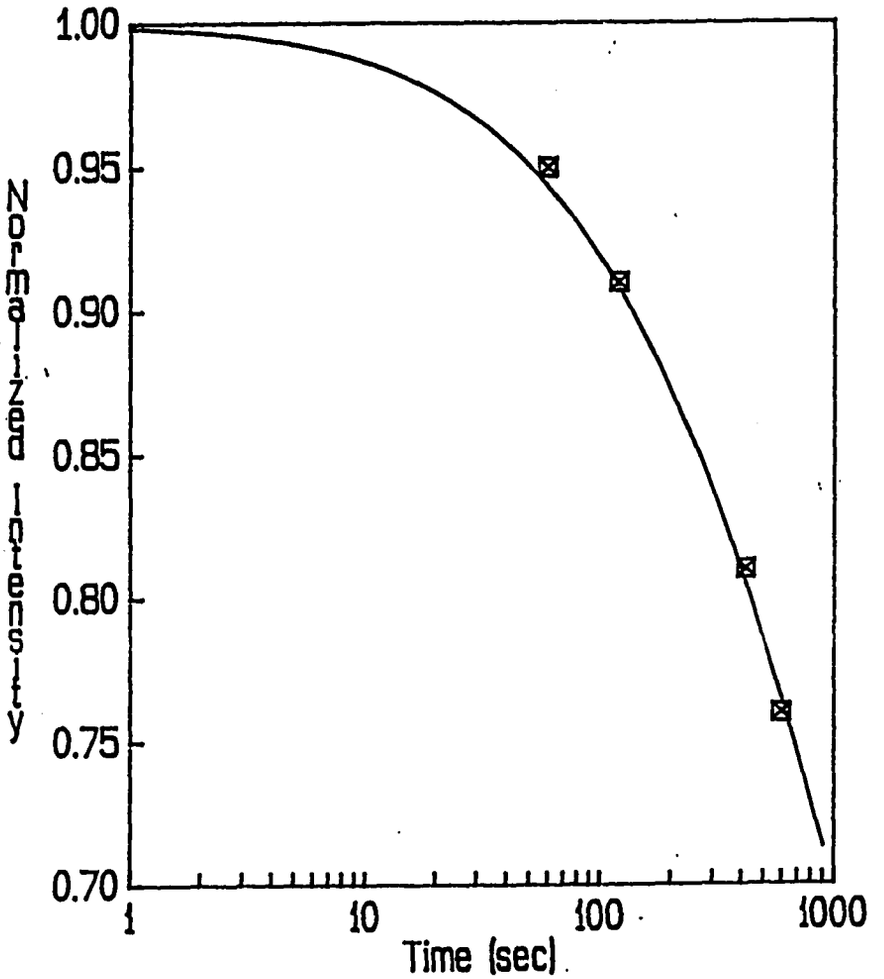
1.00
0.95
0.90
0.85
0.80
0.75
0.70
Normalized Intensity
1
10
100
1000
Time (sec)

V. DISCUSSION

The hole growth data presented provide a good test of distribution functions for the phonon-assisted tunneling rate of NPHB. The distribution function of Jankowiak *et al.* [14] (Eq. 5), like the distribution function proposed earlier [12, 55, 56], is based on a Gaussian distribution for the tunnel parameter λ and has been shown to provide a good description of the dispersive kinetics for burn fluences which vary over decades. This includes the regions of the hole growth curves which are not linear on a log t scale; linear behavior is predicted for a uniform distribution of λ when an approximate approach for evaluation of the integral in D(t), Eq. 7, is employed [8]. It should be pointed out that, when detailed analysis of hole growth kinetics is not practical, one can estimate the value of λ_0 using $\lambda_0 = -\frac{1}{2} \ln[t_{1/2}\Sigma_0]^{-1}$ [14]. Here $\Sigma_0 = P\sigma\Omega_0/k$ and $t_{1/2}$ is the burn time required to produce a hole whose depth is 50% of the saturated (maximum) hole depth. This expression is accurate for sufficiently large values of σ_2, $\gtrsim 1.5$ [14]. However, a value for λ_0 by itself is not of particular interest since it is σ_2 that determines the dispersive kinetics of NPHB which, of course, provided the motivation for the present work.

Before discussing the results, the effect of orientational averaging on the hole growth kinetics must be determined. This is necessary since, in these experiments, both the burn and probe beams (identical) were polarized. For this situation the expression for the fractional hole depth, 1 - D(t) [cf. Eq. 3], is modified to

$$\frac{1}{4\pi}\int_0^{\infty} dR\ f(R)\int_0^{2\pi} d\phi\int_0^{\pi} d\theta\ [1-\exp(-P\sigma\phi(R)t\ \cos^2\theta)]\ \cos^2\theta\ \sin\theta, \quad (9)$$

where θ is the angle between the laser polarization and transition dipole vectors and $\phi(R) \approx R/k$. Given that the square of the product of these two vectors is $\cos^2\theta$, one anticipates that the effect of orientational averaging on hole growth should be most pronounced for the latter stages of the burn. In the short burn time limit Eq. 9 can be evaluated analytically and when it is noted that

$$\frac{1}{4\pi}\int_0^{2\pi} d\phi\int_0^{\pi} d\theta\ \cos^2\theta\ \sin\theta = 1/3, \quad (10)$$

Eq. 9 reduces to 3/5 $\langle R\rangle P\sigma t/k$ for a fractional hole depth normalized so that the pre-burn absorption intensity has a value of unity. The average relaxation rate is [14]

$$\langle R\rangle = R_0\ \exp(2\sigma_2^2), \quad (11)$$

where $R_0 = \Omega_0 \exp(-2\lambda_0)$. The factor 3/5 is absent for the case of an oriented sample with all transition dipoles parallel to the laser polarization vector, which is implied in the analysis of the previous section since the value of the peak absorption cross-section used corresponds to parallel orientation. Thus, the effect of ignoring orientational averaging in the previous section is expected to be that the determined values of λ_0 should be corrected by an additive factor $[\ln (3/5)]/2 = -0.3$. This is confirmed by curve b of Fig. 13 which was calculated with Eq. 7, modified to include orientational averaging as in Eq. 9, for $\sigma_2 = 0$ and $\lambda_0 = 7.8 - 0.3 = 7.5$. This curve should be compared with curve a of Fig. 13 for $\sigma_2 = 0$ and $\lambda_0 = 7.8$ and no orientational averaging. The two curves are in close agreement to the left of the isointensity point. Orientational averaging has a significant effect on hole growth at longer times; however, it is considerably weaker than that from the R-distribution for $\sigma_2 = 0.6$, curve c of Fig. 13. The effect of orientational averaging on hole growth has been previously considered [15, 43]. However, the observation that orientational averaging is relatively unimportant for the first half of the burn is not obvious from the previous studies.

The λ_0- and σ_2- values for the systems studied are given in Table I along with the values for <R> and the

corresponding average quantum efficiency for the hole burning, $\langle\phi\rangle = \frac{\langle R\rangle}{\langle R\rangle + k}$. The values for λ_0 have not been corrected to account for orientational averaging due to the fact that the value of $\sigma = 40 \times 10^{-12}$ cm^2 used may be a lower limit due to a spectral diffusion contribution to the ZPH hole widths measured at 1.6 K, cf. Experimental section. If it is assumed that this value is too low by a factor of 4 (see Experimental), the correction to the λ_0 values is 0.7. This correction is comparable in magnitude but opposite in sign to the correction from orientational averaging.

The value of λ_0 can also be affected by spontaneous hole filling (SPHF) which is a dark ground state process that causes filling of the ZPH. The kinetics for SPHF are also dispersive [14, 18]. Spontaneous hole filling is operative for OX 720 in both glycerol and PVOH and leads to $\approx$ 10% filling in $\approx$ 100 s following termination of the burn. As reported, the SPHF kinetics for OX 720 in glycerol have been analyzed with the distribution function of Eq. 5 and values of $\lambda_0 = 18$ and $\sigma_2 = 1.5$ are determined. These values yield an average SPHF relaxation rate from Eq. 11 equal to 0.02 s^{-1} for $\Omega_0 = 10^{12}$ s^{-1} (the same value used for the hole growth kinetics). The value of 0.02 s^{-1} is about six orders of magnitude smaller than $\langle R\rangle$ for NPHB. However, the competition between hole growth and filling depends on the burn intensity and, thus, one would expect that the effect

Table I: Dispersive hole growth kinetics parameters for Oxazine 720 in different hosts at T_B = 1.6 K. The value for $\langle\phi\rangle$ was calculated with k = 3.7 x 10^8 s^{-1}. For the hole growth kinetic analysis a value of σ = 40 x 10^{-12} cm^2 was used. Also, values for SPHF are reported.

Host	λ_0	σ_2	$\langle R \rangle$ (s^{-1})	$\langle\phi\rangle$	$\langle\phi\rangle_{\zeta=0.05}$
glycerol	7.8	0.8	6.0 x 10^5	1.6 x 10^{-3}	1.5 x 10^{-2}
glycerol (deut.)	9.8	1.0	2.3 x 10^4	6.1 x 10^{-5}	7.8 x 10^{-4}
PVOH	7.6	1.0	1.85 x 10^6	5.0 x 10^{-3}	6.0 x 10^{-2}
PVOD	9.4	1.2	1.2 x 10^5	3.3 x 10^{-4}	5.1 x 10^{-2}
SPHF	18	1.5	2.1 x 10^{-2}		

of SPHF on the hole growth curve would be most pronounced for the lowest burn intensities used, i.e., nW/cm^2. However, evidence to confirm this hypothesis could not be ascertained from these studies. Thus, it is concluded that SPHF does not affect the values determined for λ_0 and σ_2.

The NPHB efficiencies reported here for OX 720 in glycerol and PVOH are higher than any reported thus far. The data of Ref. 35 for the dye molecule resorufin in glycerol indicate a somewhat lower efficiency. However, it should be noted that ionic dye molecules in hydroxylated amorphous hosts are significantly more efficient than other classes of systems studied earlier [5]. It is instructive to consider the average value of R as a function of the fractional hole depth ζ, $\langle R \rangle_\zeta$. Recall that the average value of R is defined as

$$\langle R \rangle \equiv \frac{\int_0^\infty dR\ R\ f(R)}{\int_0^\infty dR\ f(R)} \tag{12}$$

where f(R) is described in Eq. 5. A similar definition is made for $\langle R \rangle_\zeta$ with the lower limits of integration being R_{min} where $R_{min} > 0$. The denominator of Eq. 12 is ζ and it is easily shown that $\zeta = g(\infty) - g(y_{min})$ where

$$g(x) = \sqrt{\frac{1}{2\pi}} \int_0^x dx\ \exp(-x^2/2) \tag{13}$$

and

$$y_{min} = \frac{\ln \frac{R_{min}}{\Omega_0}}{2\sigma_2} + \frac{\lambda_0}{\sigma_2}. \qquad (14)$$

The desired result is

$$\langle R \rangle_\zeta = \frac{\langle R \rangle}{\zeta} [0.5 - g(t)], \qquad (15)$$

where $t = y_{min} - 2\sigma_2$; y_{min} is determined by the fractional hole depth using $g(y_{min}) = 0.5 - \zeta$. Equation 15 is valid for $\lambda_0/\sigma_2 \gg 1$ (which is satisfied for the systems studied here). The quantum yield for burning to a hole depth of ζ can be defined as $\langle \phi \rangle_\zeta = \frac{\langle R \rangle_\zeta}{\langle R \rangle_\zeta + k}$.

The ratio of $\langle R \rangle_\zeta$ to $\langle R \rangle$ is plotted in Fig. 20 for OX 720 in glycerol. All points are normalized to $\zeta = 0.0004$ with $\langle R \rangle_{0.0004}/\langle R \rangle = 100$. It can be seen, for example, that the quantum efficiency $\langle \phi \rangle$ for a fractional hole depth of 0.01 is $\approx 4 \times 10^{-2}$.

The effect of deuteration of the host hydroxyl protons on the OX 720 hole growth kinetics is now considered. The data in Table I yield values of 60 and 40 for R_0^H/R_0^D for glycerol and polyvinyl alcohol, respectively (see Eq. 11). Although significant, the effect of deuteration is not as large as expected for a tunneling coordinate involving only proton motion. From Table I one obtains $\lambda_0^D/\lambda_0^H = 1.26$ and

Figure 20: Relative hole burning quantum efficiency plotted as a function of the fractional hole depth ζ. Calculations performed with $\lambda_0 = 7.8$ and $\sigma_2 = 0.8$ and σ, Ω_0 and k values given in Fig. 9 caption. All points are normalized to $\zeta = 0.0004$ with $\langle R \rangle_\zeta / \langle R \rangle$ for this ζ-value equal to 100. See text for discussion. $\langle R \rangle_\zeta$ values for $\zeta = 0.05$ are given in Table I

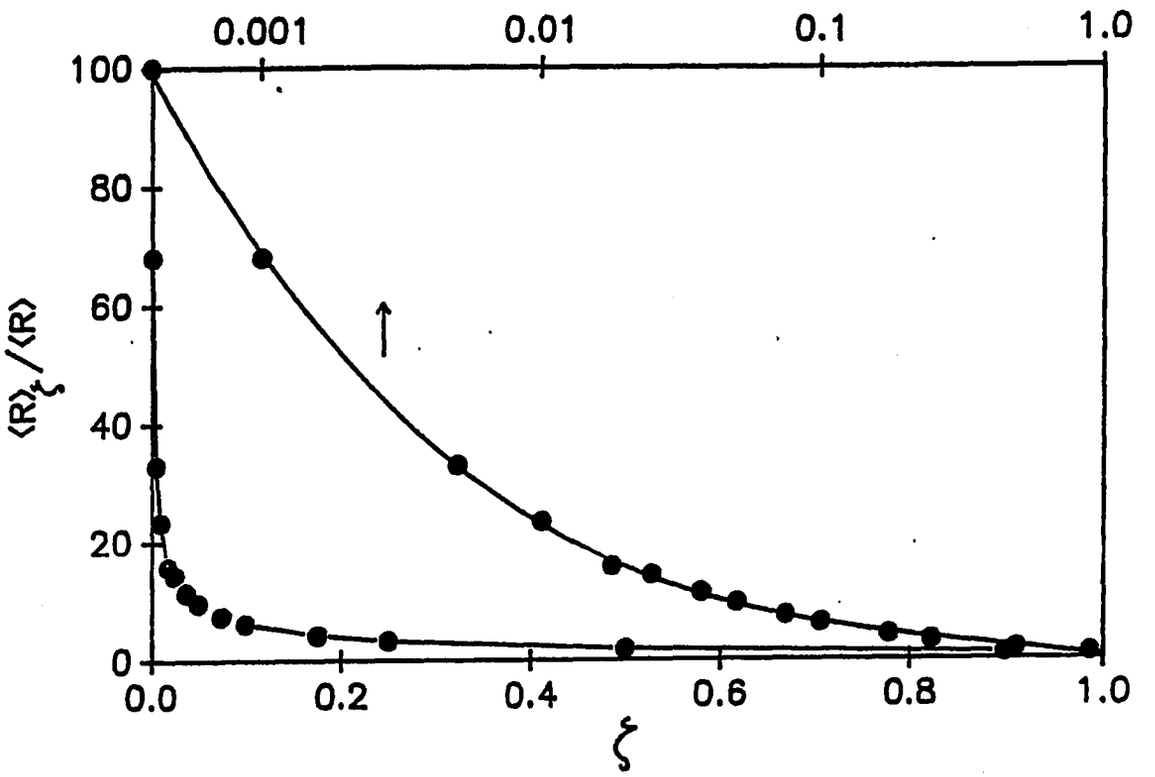
0.001
0.01
0.1
1.0
100
80
60
40
20
0
0.0
0.2
0.4
0.6
0.8
1.0
$\langle R \rangle_\zeta / \langle R \rangle$
ζ

1.24 for glycerol and polyvinyl alcohol, values which are identical within experimental uncertainty and less than $\sqrt{2}$ for pure proton tunneling. It should be noted that the λ_0^D values were determined under the assumption that $\Omega_0^D = \Omega_0^H = 10^{12}\ s^{-1}$. With reference to Eq. 2 and the accompanying expression for Ω_0 in the text, one observes that $\Omega_0 \propto \omega_0^2$, where ω_0 is the harmonic frequency for the wells of the TLS. Thus for pure proton tunneling, $\Omega_0^D = \frac{1}{2}\Omega_o^H$. For such tunneling the tabulated λ_0^D values would be subject to an additive correction of $\frac{1}{2}\ln(\frac{1}{2}) = -0.3$ ($<R>^D$ is not affected). This would reduce the above values for λ_0^D/λ_0^H to 1.2.

Unfortunately the absence of detailed structural information on hydrogen bonding in the OX 720 inner shell region permits only speculative remarks about the hydrogen bond rearrangements involved in NPHB. Of course, the existence of a distribution for the relaxation rate R and the fact that the blue-shifted anti-hole, Fig. 4, is extremely broad means that the "reaction" coordinate cannot be precisely defined. Nevertheless, from the structure of OX 720, Fig. 8, one identifies the positively charged nitrogen of the iminium ion as the entity capable of forming the strongest intermolecular hydrogen bond with the hydroxyl group oxygen. The situation is analogous to that for resorufin in ethanol, a system whose NPHB properties have been studied by Kokai *et al.* [57]. The electronic structure of

resorufin is similar to that of OX 720 with the major difference being the replacement of the iminium ion by the negatively charged alkoxide ion and replacement of the ethyl amino group by the carbonyl oxygen moiety (resorufin possesses the central phenoxazine ring but not the benzene ring fused to the ring attached to the iminium ion). Kokai *et al.* [57] have determined that the hole burning efficiency in the mixed host ethanol/ethanol-d depends quadratically on the ethanol concentration and draw the reasonable conclusion that the mechanism of NPHB for resorufin involves the concerted rearrangement of two hydrogen bonds. One possibility they suggest is hydrogen bond switching between the alkoxide ion and two neighboring ethanol molecules. Another stems from the two resonance structures for resorufin in which the positions of the alkoxide ion and carbonyl oxygen (analogous to the iminium ion and ethyl amino group) are interchanged. In the glass the Na^+ counter ion can produce an energetic inequivalence between these two resonance structures for both the ground and excited electronic states. The counterpart for OX 720 is the perchlorate ion, ClO_4^-. For the electronic resonance structure interpretation, motion of the atoms of the skeletal ring system must be taken into account in addition to the motion of the hydroxyl protons. The possibility that the mechanism is one that involves concerted H-bond

rearrangement of host molecules which are not involved in bonding to the probe is also considered in Ref. 54. Electronic excitation of the probe could conceivably trigger a greater degree of linearity in the hydrogen bonds. Although polarized hole burning studies of the entire hole profile (ZPH, phonon sideband holes and anti-hole) of OX 720 have not been performed, it is thought unlikely that OX 720 undergoes significant displacement (rotation) during the hole burning process at 1.6 K. Such studies have been performed for another laser dye, cresyl violet, in PVOH [53] and chlorophyll a in the core antenna complex of photosystem I [56]. For both systems the polarization ratios of the holes and anti-hole are consistent with insignificant probe molecule rotation at 1.6 K.

In principle one can estimate the average barrier height $\langle V^{\beta} \rangle$ for the excited state TLS^{β}_{ext} from Gamov's formula [59]

$$\langle V^{\beta} \rangle = \frac{\lambda_0^2 \hbar^2}{2md^2} \qquad (16)$$

where d is the average distance between potential energy minima and m is the tunneling mass. For the purpose of a rough calculation let d = 1 Å (which is close to the value for hydrogen bond rearrangement in the benzoic acid crystal [60]). From the observation that $\lambda_0^D/\lambda_0^H \approx 1.25$, introduce a fictitious hydrogen-like particle with m ≈ 1.7 (isotope m ≈

2.7). One then obtains $\langle V^{\beta} \rangle \approx 600$ cm^{-1}. Other groups have made estimates for $\langle V^{\alpha} \rangle$ for the ground electronic state, TLS^{α}_{ext} [8, 61-63]. For example, Friedrich and Haarer [8] estimate a value for quinizarin in ethanol of several thousand cm^{-1}. Of course, given the long persistence time of the hole one would expect, on the basis of the TLS model, that the excited state barrier height should be significantly smaller than for the ground state. As stated earlier, the value of λ_0 for spontaneous filling (OX 720/glycerol) is 18. If it is assumed that the filling is simply a consequence of "reverse" tunneling in each and every TLS^{α}_{ext} of the static distribution, then $\langle V^{\alpha} \rangle \approx 3000$ cm^{-1}. Although these numbers should not be taken too seriously, it is interesting that the average barrier heights are greater than the glass transition temperature of glycerol (~ 180 K) as was previously noted by Friedrich and Haarer [8].

Consider now the temperature independence of the hole burning efficiencies for OX 720 in glycerol (1.6 - 7 K). Recently, Elschner and Bässler [62] have reported that the hole burning efficiency for cresyl violet in glycerol is constant over a much broader temperature range. On the surface these results would seem to be consistent with the simple TLS model. However, polarized hole burned spectra as a function of T_B for cresyl violet in PVOH and chlorophyll a

in the core antenna complex of photosystem I have recently been obtained which indicate that such a conclusion need not be valid [53, 58]. For both systems the polarization data for the ZPH, phonon sideband holes and anti-hole indicate that no significant rotation of the probe molecule accompanies hole burning at low temperatures ($\lesssim$ 6 K) while at higher temperatures (by 15 K) significant rotation does occur. Such a finding is not consistent with a static distribution of TLS_{ext} for a single coordinate, cf. Fig 1. However, and as mentioned earlier, the hole burning efficiency of cresyl violet in PVOH is not dependent on T_B. This suggests that the T_B dependence of the polarization of the entire hole profile plus anti-hole may allow for more stringent testing of the simple TLS model than that of the hole growth kinetics.

Finally, it is noted that Jankowiak and Small have extended the utilization of the Gaussian distribution function to the TLS asymmetry parameter Δ and derived distribution functions for W^2 and Δ^2. The latter functions were first used to obtain an analytic expression for the TLS density of states $\rho(E)$, where E is the tunnel state splitting ($E^2 = W^2 + \Delta^2$) [9]. Following that it was shown that they lead to more accurate configurational averaging for the optical dephasing frequency [30]. Perhaps the most notable achievement with these distribution functions has

been the demonstration that, for vitreous silica, the temperature power laws for the specific heat, thermal conductivity and optical dephasing as well as the gap in $\rho(E)$ at very low energy can be understood with one and the same set of distribution function parameter values [30, 40, 41, 63, 64]. Also note that the recent results of Littau *et al.* [65] on spectral diffusion offer additional support for the utility of the R-distribution function utilized here.

VI. CONCLUSIONS

The dispersion introduced into the kinetics of dynamical processes by the structural disorder of amorphous solids is of wide ranging interest. Nonphotochemical hole burning (NPHB) provides an important approach for the study of dispersive kinetics and, in particular, those of phonon-assisted tunneling. The zero-phonon hole (ZPH) growth data of OX 720 in glycerol and PVOH presented here span 5 decades of burn fluence (burn intensities of nW - $\mu W/cm^2$). It was found that the distribution function of Jankowiak *et al.* (Eq. 5) for the NPHB rate R allows for a good description of the kinetics. The distribution function, f(R), is based on the reasonable assumption that the dispersion is due predominantly to the distribution of the tunnel parameter λ, which is taken to be a Gaussian (width = $2^{3/2}$ $(\ln 2)^{1/2}$ σ_2). In contrast with previous studies, the analysis takes into account the electron-phonon coupling (Huang-Rhys factor S), albeit in an approximate way (which, nevertheless, is quite accurate for weak coupling, *vide infra*). Failure to do so is less than satisfactory since one is not able to determine the extent to which the residual absorption at ω_B in the long burn time limit is contributed to by gross heterogeneity.

The OX 720 systems studied have the highest known NPHB efficiencies, cf. Table I. Average quantum yields, $\langle\phi\rangle$, are 2×10^{-3} and 5×10^{-3} for glycerol and PVOH. Even though the σ_2 values (≈ 1) are not so large, the effects of dispersion are very apparent. For example, the quantum yields associated with a hole of fractional depth $\zeta = 0.05$ are a factor of 10 higher than $\langle\phi\rangle$. The $\langle R\rangle_\zeta/\langle R\rangle$ versus ζ plot of Fig. 20 (calculated with Eq. 15) illustrates the strong dispersion of hole growth which results from the λ distribution.

The finding that the dependence of the ZPH growth kinetics on the burn temperature (T_B) in the 1.6 - 7.0 K range can be accounted for by the temperature dependence of the induced absorption rate (pure dephasing) is interesting. A similar finding was noted to have been reported for two other systems, but over a wider temperature range (1.6 - 15.0 K for cresyl violet in PVOH [53]). The implications are as follows: first, the phonon-assisted tunneling mechanism for hole burning is dominant for said range of T_B, i.e., barrier hopping is not important; and tunneling in the excited state occurs from higher to lower energy configurations. One does expect that barrier hopping should become important at sufficiently high temperature and that this temperature should depend on the probe-host system. It is the second implication that is surprising, especially

when it is recalled that these results show that 100% of the zero-phonon lines coincident with ω_B can be burned. There is little likelihood that 100% hole burning would not be observed in the limit as $T_B \rightarrow 0$ K. It is not possible to reconcile these findings and others [24] in terms of the simple TLS_{ext} model, with its implied democratic energetic dispositions of the "precursor" and "product" wells for the ground and excited probe molecule states. Random statistical distributions lead to the prediction that only 50% of the ZPL should be burned in the limit as $T_B \rightarrow 0$ K. It is necessary, therefore, to go beyond the TLS_{ext} model with its implied static distribution. Shu and Small have done so by proposing a mechanism for NPHB based on a hierarchy of constrained dynamical events [24].

At least for $\pi\pi^*$ states, NPHB is particularly facile for polar hydrogen bonding hosts. As a class, ionic dye molecules in such hosts appear to be most efficient. The deuteration studies reported herein establish again that, for this class, the NPHB coordinate is quite localized with significant amplitude of motion for the proton of the host hydroxyl groups. In sharp contrast, earlier work has shown that pure dephasing is, at best, only weakly dependent on deuteration. Thus, the tunneling coordinates associated with dephasing are significantly more delocalized than those associated with the rate determining step of NPHB.

The expression for the fractional ZPH depth 1 - D(t), with D(t) given by Eq. 3, does not take into account the linear electron-phonon coupling. The modifications to do so are quite straightforward [46, 66] and include incorporation of the single site absorption profile (ZPL plus one- and multi-phonon sidebands) and site excitation distribution function. For strong coupling (S > 1), the only reliable approach to the characterization of the dispersive kinetics would involve monitoring of the entire hole profile (ZPH plus phonon sideband holes). Interference from the anti-hole would have to be taken into account [24, 66]. Furthermore, it would be necessary to study hole growth as a function of ω_B within the inhomogeneously broadened profile. Obviously, it is far simpler to study systems with weak coupling. For such systems and with the experimental methodology reported, the ZPH is not significantly interfered with by the phonon sideband holes up to the point of its saturation. An independent measurement of S allows for the determination of the ZPL Franck-Condon factor exp(-S) (accurate for ω_B located on the low energy side of the absorption origin profile [46, 66]). In the absence of gross heterogeneity this factor is the maximum fractional ZPH depth. The Franck-Condon factor must also be taken into account in the calculation of the peak absorption cross-section of the ZPL. Thus, knowledge of S enables the

VII. REFERENCES

1. P. W. Anderson, B. I. Halperin and C. M. Varma, Philos. Mag. 25 (1972) 1.

2. W. A. Phillips, J. Low Temp. Phys., 7 (1972) 351.

3. W. A. Phillips, editor, *Amorphous Solids - Low Temperature Properties*, (Springer-Verlag, Berlin, 1981).

4. S. Hunklinger and A. K. Raychaudhuri, in *Progress in Low Temperature Physics*, edited by D. F. Brewer (North-Holland, Amsterdam, 1986), Vol. IX, Chap. 3, p. 265.

5. J. M. Hayes, R. Jankowiak and G. J. Small, in *Topics in Current Physics, Persistent Spectral Hole Burning: Science and Applications*, edited by W. E. Moerner (Springer-Verlag, New York, 1987), Chap. 5 and other chapters therein.

6. S. K. Lyo, in *Electronic Excitation and Interaction Processes in Organic Molecular Aggregates*, Vol. 49 of *Solid State Science*, edited by P. Reinecker, H. Haken and H. C. Wolf (Springer-Verlag, Berlin, 1983), p. 215.

7. Y. S. Bai and M. D. Fayer, Comments Cond. Mat. Phys. 14 (1989) 343.

8. J. Friedrich and D. Haarer, in *Optical Spectroscopy of Glasses*, edited by I. Zschokke (Reidel Publishing Company, Dordrecht, Holland, 1986), p. 149.

9. R. Jankowiak, G. J. Small and K. B. Athreya, J. Phys. Chem. 90 (1986) 3890 and references therein.

10. S. K. Lyo and R. Orbach, Phys. Rev. B 22 (1980) 4223.

11. J. M. Hayes, R. P. Stout and G. J. Small, J. Chem. Phys. 74 (1981) 4266.

12. R. Jankowiak, R. Richert and H. Bässler, J. Chem. Phys. 89 (1985) 4569.

13. A. Elschner and H. Bässler, Chem. Phys. 112 (1987) 285.

14. R. Jankowiak, L. Shu, M. J. Kenney and G. J. Small, J. Lum. 36 (1987) 293.

15. A. Elschner and H. Bässler, Chem. Phys. 123 (1988) 305.

16. W. Köhler, J. Meiler and J. Friedrich, Phys. Rev. B 35 (1987) 4031.

17. W. Köhler and J. Friedrich, Phys. Rev. Letters 59 (1987) 2199.

18. R. Jankowiak and G. J. Small, Science 237 (1987) 618.

19. H. P. Trommsdorf, J. M. Ziegler and R. M. Hochstrasser, J. Chem. Phys. 89 (1988) 4440.

20. J. S. Shirk, R. Pong and A. W. Snow, J. Chem. Phys. 90 (1989) 3380.

21. J. M. Hayes and G. J. Small, Chem. Phys. 27 (1978) 151.

22. J. M. Hayes and G. J. Small, Chem. Phys. Lett. 54 (1978) 435.

23. V. Bogner and R. Schwarz, Phys. Rev. B 24 (1981) 2846.

24. L. Shu and G. J. Small, Chem. Phys. 141 (1990) 447.

25. W. Köhler, J. Friedrich, R. Fischer and H. Scheer, J. Chem. Phys. 89 (1988) 871.

26. S. G. Johnson and G. J. Small, Chem. Phys. Lett. 155 (1989) 371.

27. J. K. Gillie, G. J. Small and J. H. Golbeck, J. Phys. Chem. 93 (1989) 1620.

28. A. F. Childs and A. H. Francis, J. Phys. Chem. 89 (1985) 466.

29. R. Jankowiak and H. Bässler, J. Mol. Electron. 1 (1985) 73.

30. R. Jankowiak, G. J. Small and B. Ries, Chem. Phys. 118 (1987) 223.

31. J. E. Grabner, L. C. Allen, B. Golding and A. B. Kane, Phys. Rev. B 27 (1983) 3637.

32. H. Tadokoro, Bull. Chem. Soc. Jpn. 32 (1959) 1252.

33. H. Tadokoro, S. Seki and I. Nitta, J. Polym. Sci. 22 (1956) 563

34. H. Tadokoro, H. Nagai, S. Seki and I. Nitta, Bull. Chem. Soc. Jpn. 34 (1961) 1504.

35. B. L. Fearey, T. P. Carter and G. J. Small, J. Phys. Chem. 87 (1983) 3590.

36. T. P. Causgrove and W. S. Struve, Ames Laboratory - USDOE, (1986) unpublished results.

37. M. Berg, C. A. Walsh, L. R. Narasimhan, K. A. Littau and M. D. Fayer, J. Chem. Phys. 88 (1988) 1564.

38. C. A. Walsh, M. Berg, L. R. Narasimhan, and M. D. Fayer, Chem. Phys. Lett. 139 (1987) 485.

39. R. van den Berg and S. Völker, Chem. Phys. Lett. 137 (1985) 1.

40. R. Jankowiak and G. J. Small, Chem. Phys. Lett. 128 (1986) 377.

41. R. Jankowiak and G. J. Small, J. Phys. Chem. 90 (1986) 5612.

42. P. Reichert and R. Schilling, Phys. Rev. B 32 (1985) 5731.

43. W. Köhler and J. Friedrich, Chem. Phys. Lett. 134 (1987) 200.

44. There is an interference between the pseudo-phonon sideband hole and the real phonon sideband hole which leads to a distortion of the real anti-hole shape (see Ref. 24).

45. J. M. Hayes and G. J. Small, J. Phys. Chem. 90 (1986) 4928.

46. J. M. Hayes, J. K. Gillie, D. Tang and G. J. Small, Biochim. Biophys. Acta 932 (1988) 305.

47. S. G. Johnson, D. Tang, R. Jankowiak, G. J. Small and D. M. Tiede, J. Phys. Chem. 93 (1989) 5953.

48. S. G. Johnson, D. Tang, R. Jankowiak, J. M. Hayes, G. J. Small and D. M. Tiede, J. Phys. Chem. in press.

49. R. Jankowiak, D. Tang, G. J. Small and M. Siebert, J. Phys. Chem. 93 (1989) 1649.

50. J. K. Gillie, G. J. Small and J. H. Golbeck, J. Phys. Chem. 93 (1989) 1620.

51. B. L. Fearey, R. P. Stout, J. M. Hayes and G. J. Small, J. Chem. Phys. 78 (1983) 7013.

52. H. Hardle, G. Weiss, S. Hunklinger and F. Baumann, Z. Phys. B – Condensed Matter 65 (1987) 291.

53. L. Shu and G. J. Small, to be published.

54. S. Völker, in *Relaxation Processes in Molecular Excited States*, edited by J. Fünfschilling (Kluwer Academic Publ., Amsterdam, 1989), p. 113.

55. A. Elschner, R. Richert and H. Bässler, Chem. Phys. Lett. 127 (1986) 105.

56. R. Richert, J. Chem. Phys. 86 (1987) 1743.

57. F. Kokai, H. Tanaka, J. I. Brauman and M. D. Fayer, Chem. Phys. Lett. 143 (1988) 1.

58. I.–J. Lee, P. A. Lyle and G. J. Small, to be published.

59. For example, see A. S. Davydov, *Quantenmechanik*, VEB Deutsches Verlag der Wissenschaften, Berlin (1970).

60. H. P. Trommsdorf, in *Proceedings of the Academy of Sciences of the Estonian SSR*, Physics, Mathematics 37 (1988) 166.

61. W. Köhler, J. Meiler and J. Friedrich, Phys. Rev. B 35 (1987) 4031.

62. A. Elschner and H. Bässler, J. Lum., in press.

63. R. Jankowiak and G. J. Small, Phys. Rev. B 37 (1988) 8407.

64. R. Jankowiak, J. M. Hayes and G. J. Small, Phys. Rev. B 38 (1988) 2084.

65. K. A. Littau, Y. S. Bai and M. D. Fayer, Chem. Phys. Lett. 159 (1989) 1.

66. I.–J. Lee, J. M. Hayes and G. J. Small, J. Chem. Phys. 91 (1989) 3463.

67. P. J. Davis and I. Polonsky, in *Handbook of Mathematical Functions*, edited by M. Abramowitz and I. A. Stegun (Dover Publications, New York, 1965), p. 886.

VIII. ACKNOWLEDGEMENTS

Any person who has completed their graduate career is aware that graduate school is not a solitary venture. There are many individuals who have helped me during my own graduate school tenure and I take this opportunity to thank them for their support.

First, I wish to thank Dr. Gerald Small for his advice, encouragement and patience during the past several years. I have learned many things from Dr. Small, but one lesson stands out above the others. He told me to remember one thing when presenting any information to a group; be sure that when the presentation is completed, the persons in the room leave having learned something that they did not know before they came. I have tried to follow this advice in all presentations since that time. I only hope that I have been successful.

In addition, I want to thank Dr. John Hayes and Dr. Ryszard Jankowiak. Through these two individuals I have seen the joy of discovery and the perseverance needed to succeed.

The friends I have met during graduate school are people I will always remember. Kevin Gillie, Steve Johnson,

Bryan Isaac and Patrice Christiansen shared many laughs and even a few tears. Joel Kress helped me in class and on the hockey rink. And, In-Ja Lee and Luchuan Shu never stopped questioning the why and how, providing me with practice for my career as a teacher

Tom Carter is a friend who must stand out from the others. He helped me get started and showed me how to do research. His advice, both personal and professional, has proved to be excellent. I look forward to many more family gatherings with him and his family, Linda and Beth.

I especially want to thank my own family for their support. My mother and father gave me the fortitude to embark on this path and the stubbornness to continue. They were my first and most influential teachers.

Finally, and most importantly, I want to thank Margaret, my wife. She helped me survive when I did not think that I could. She kept faith in me, even when I began to lose faith in myself. She kicked me in the butt when I needed it and patted me on the back when I earned it. If Margaret had not been there, I would not have succeeded. I only hope that I can repay her someday.

IX. APPENDIX A: FORTRAN COMPUTER PROGRAMS FOR DATA ACQUISITION

```
      PROGRAM SCANNR
C
C     THIS PROGRAM WILL SCAN THE RING LASER, COLLECT DATA
C     FROM THE ITHACO INTEGRATOR AND STEP THE CHART RECORDER
C
      IMPLICIT REAL (A-H,O-Z), INTEGER (I-N)
      LOGICAL*1 COM(1)
      CALL IBINIT                !INITIALIZE THE INTEGRATOR
5     CALL DAOUTP(3,3072)        !SET LASER TO START OF SCAN
      CALL DAOUTP(4,0)           !MAKE SURE SHUTTER IS CLOSED
C
      CALL PRINT('DO YOU WANT TO BURN(B), SCAN(S), ALIGN(A),
      1 OR EXIT(E)?')
      READ (5,898) COM(1)

      IF (COM(1).EQ.'S') CALL SCAN
      IF (COM(1).EQ.'B' .OR. COM(1).EQ.'A') CALL BURN(COM)
      IF (COM(1).EQ.'E') GOTO 999

      GOTO 5

999   STOP
898   FORMAT(A1)

      END
```

```
      SUBROUTINE SCAN

      IMPLICIT REAL (A-H,O-Z), INTEGER (I-N)

      NSTEP=0
      CALL OPENER                !GET DATA FILE NAME
      VOLTS = -5.                !INITIALIZES SCAN VOLTAGE

      CALL PRINT('ENTER NUMBER OF GHz TO BE SCANNED.')
      ACCEPT *,IRANGE
      CALL PRINT('CHART SCALE IS 2 GHz/cm')

      NPTS = IRANGE * 50         !CALCULATES NUMBER OF DATA
C                                !POINTS ASSUMING 50 POINTS
C                                !ACROSS A 1 GHz WIDE HOLE

      STEP = 10. / NPTS          !CALCULATES SIZE OF VOLTAGE STEP
      CALL PRINT('ENTER OD MAX (ANY REAL NUMBER)')
      ACCEPT *,GAIN
      aGAIN=4096./GAIN
      CALL PRINT('ENTER REAL TIME OFFSET (IN OD UNITS)')
      ACCEPT *,OFFSET
      CALL CHART(ISCALE)         !SET CHART RECORDER PARAMETERS
      CALL DAOUTP(4,4)           !OPEN THE SHUTTER
      DO 33 L=1,100              !WAIT FOR SHUTTER TO OPEN
C                                !COMPLETELY
33    CONTINUE
      DO 10 I=1,NPTS
         NCOUNT=NCOUNT+1                  !WRITE DATA COUNTER
         IVALUE = 2048-(204.8*VOLTS)      !CALCULATES VALUE TO BE
C                                         !OUTPUT AT THE D/A TO
C                                         !STEP THE LASER
         CALL DAOUTP(3,IVALUE)            !STEPS THE LASER
         CALL IBDAT(OFFSET,aGAIN,ncount)
         VOLTS = VOLTS + STEP             !INCREMENTS LASER STEP
         IF (NCOUNT.EQ.256) CALL WRTDAT(NCOUNT)
         CALL PEN                         !STEP THE CHART RECORDER
10       CONTINUE
      CALL DAOUTP(4,0)                    !CLOSE THE SHUTTER
      DO 34 L=1,100                       !WAIT FOR SHUTTER TO
C                                         !CLOSE COMPLETELY
34    CONTINUE
      CALL DAOUTP(3,3072)                 !RESET THE LASER
      IF (NCOUNT.GT.0) CALL WRTDAT(NCOUNT)
      CLOSE (UNIT=1)
      CALL SPACE                    !PUT A SPACE BETWEEN SCANS
      RETURN
      END
```

```
      SUBROUTINE BURN(COM)

C     THIS ROUTINE WILL OPEN THE SHUTTER FOR EITHER A
C     SPECIFIED OR AN INDEFINITE PERIOD OF TIME.  THE PURPOSE
C     OF THE ROUTINE IS TO ENABLE COMPUTER CONTROL OF THE
C     LENGTH OF THE BURN.  IN ADDITION, IT WILL ALLOW
C     THE USER TO OPEN OR CLOSE THE SHUTTER WITHOUT
C     DISCONNECTING THE LASER.  THIS SHOULD BE USEFUL DURING
C     ALIGNMENT.
C     I HAVE NOW ADDED THE ABILITY TO BURN MULTIPLE HOLES.

      IMPLICIT REAL (A-H,O-Z), INTEGER (I-N)
      LOGICAL*1 COM(1)
      DIMENSION IHOL(11),TIME(11)

      IF (COM(1) .EQ. 'B') GOTO 205
      GOTO 210
205   CALL PRINT('HOW MANY HOLES DO YOU WANT TO BURN?')
      ACCEPT *,NUMHOL
      CALL PRINT('WHERE DO YOU WANT TO BURN THE HOLES?')
      CALL PRINT('0=LOW ENERGY SIDE, 50=CENTER,
     1            100=HIGH ENERGY SIDE')
      CALL PRINT('ENTER IN ORDER YOU WISH TO BURN')
      DO 10 I=1,NUMHOL
10    ACCEPT *,IHOL(I)
      CALL PRINT('HOW LONG IN SEC DO YOU WANT
     1           TO BURN EACH HOLE?')
      DO 20 I=1,NUMHOL
20    ACCEPT *,TIME(I)
      DO 30 I=1,NUMHOL
         IMIN = TIME(I) / 60              !CALCULATE BURN TIME
         ITIC = (TIME(I) - (IMIN*60)) * 60
         JPOS = 3072 - (IHOL(I) * 20.48)
         CALL DAOUTP(3,JPOS)              !GOTO BURN LAMBDA
         CALL DAOUTP(4,4)                 !OPEN THE SHUTTER
         CALL ISLEEP(0,IMIN,0,ITIC)       !WAIT FOR BURN TIME
30       CONTINUE
      CALL DAOUTP(4,0)                    !CLOSE THE SHUTTER
      RETURN

C     THIS IS THE ALIGNMENT ROUTINE

210   CALL DAOUTP(4,4)                    !OPEN THE SHUTTER
      PAUSE 'PRESS RETURN WHEN READY'
      CALL DAOUTP(4,0)                    !CLOSE THE SHUTTER
      RETURN
      END
```

```
      SUBROUTINE WRTDAT(NCOUNT)

      COMMON NREC/BLK1/ IDATA(260)
      WRITE (1'NREC)(IDATA(I),I=1,256)
      DO 1001 I=1,260
1001  IDATA(I)=0
      NCOUNT=0
      RETURN
      END
```

```
      SUBROUTINE OPENER

      LOGICAL*1 NAMF(14)
      COMMON NREC
800   WRITE(7,926)                          !GETS SIGDATA FILE NAME
      READ (5,927) NAMF
      OPEN(UNIT=1,NAME=NAMF,TYPE='OLD',FORM='UNFORMATTED'
     1     ,ERR=802)
      CLOSE(UNIT=1)
      CALL PRINT('FILE NAME ALREADY IN USE')
      GOTO 800
802   OPEN(UNIT=1,NAME=NAMF,TYPE='NEW',FORM='UNFORMATTED',
     1ACCESS='DIRECT',ASSOCIATEVARIABLE=NREC,RECORDSIZE=128,
     2ERR=1000)
      nrec=1
888   RETURN
926   FORMAT(X,'ENTER SIGNAL OUTPUT FILE NAME:',$)
927   FORMAT(14A1)
1000  CALL PRINT('BAD FILE SPEC, TRY AGAIN')
      GOTO 800
      END
```

```
      SUBROUTINE IBINIT
c     This routine sets up the parameters of the integrator
c     and allows the user to change LIA gain settings and the
c     number of integrator time periods (1 period = 1/60 sec)
c     to sample the signal for.
c
c     The initial set up is as follows:
c     A1 -> 10v full scale sensitivity
c     B0 -> 2 Hz bandwidth when Auto-Gain is x100
c     R1 -> Autorange delay 1/60 sec.
c     TB -> Trigger integration start from the computer bus
c     OC -> Continuous output mode (read data after trigger)
c     MA -> Send data in ASCII format
c     D3 -> (combined D1 and D2) integrator returns values
c           for channel A and channel B to the computer when
c           asked for data
c     S0 -> disable service request (interrupts) operation
c
      LOGICAL *1 MESSAG(50)
      COMMON/SUB1/JANS
      CALL IBIFC                  !THIS CLEARS THE INSTRUMENT BUS
      CALL IBSDC(1)               !THIS CLEARS THE INTEGRATOR
      CALL IBSEND('A1B0R1TBOCMAD3S0',-1,1) !send parameters
      MESSAG(1)=13
      CALL IBSEOI(MESSAG,1,1)
8     MESSAG(1)=63                ! ask
      MESSAG(2)=13                ! for
      CALL IBSEOI(MESSAG,2,1)     ! parameter string
      N=IBRECV(MESSAG,50,1)       ! receive parameter string
      WRITE(7,1000)
1000  FORMAT(/X,'THE INTEGRATOR PARAMETERS ARE : ')
      WRITE(7,1001) (MESSAG(I),I=1,N-1)    !write parameters
1001  FORMAT(X,50A1)
      WRITE(7,1002)
1002  FORMAT(X,'DO YOU WANT TO MAKE ANY CHANGES? (Y,N) : ',$)
      CALL YORN
      IF(JANS.EQ.0)RETURN
9     WRITE(7,1003)
1003  FORMAT(X,'ENTER PARAMETERS (DON'T USE SPACES) :',$)
      READ(7,1004)NCHAR,MESSAG          !accept parameters
1004  FORMAT(Q,50A1)
      IF(NCHAR.GT.50)GO TO 10
      CALL IBSEND(MESSAG,NCHAR,1)       !send parameters
      CALL IBSEOI(15,1,1)
      GO TO 8
10    WRITE(7,1005)
1005  FORMAT(X,'MESSAGE TOO LONG, 50 CHARACTERS TOTAL,
     1     TRY AGAIN!!!')
```

```
      GO TO 9
      END
      SUBROUTINE CHART(ISCALE)

      LOGICAL*1 E1(1)

      E1(1)=0
1     write(7,54)
54    format(x,'ENTER O.D. SCALE FACTOR'/x,
     1      '(divide O.D. by this to get the full scale O.D.
     2       of the real time output)'/x,
     3      '(use values: 1,2,5,10,20,50,100) :',$)
      READ(5,55)ISCALE
55    FORMAT(I3)

C     THE NUMBERS IN THE FOLLOWING LINES OF DATA ARE ASCII
C     VALUES OF VARIOUS KEYBOARD ELEMENTS.  THE OMNISCRIBE
C     OWNERS MANUAL CONTAINS A LIST OF THE MEANING OF EACH
C     ELEMENT.

      IF(ISCALE.EQ.1)E1(1)=101
      IF(ISCALE.EQ.2)E1(1)=102
      IF(ISCALE.EQ.5)E1(1)=103
      IF(ISCALE.EQ.10)E1(1)=104
      IF(ISCALE.EQ.20)E1(1)=105
      IF(ISCALE.EQ.50)E1(1)=106
      IF(ISCALE.EQ.100)E1(1)=107
      IF(E1(1).NE.0)GO TO 2
      WRITE(7,32)
32    FORMAT(X,'ILLEGAL EXPANSION FACTOR, TRY AGAIN')
      GO TO 1
2     imode=1
      call onrec(imode)
      write(7,98)E1(1)
98    format(X,'333qs',1a1,$)
      imode=0
      call onrec(imode)
      PAUSE 'SET PEN TO A MAJOR DIVISION AND ADJUST ZERO'
      imode=1
      call onrec(imode)
      write(7,500)
500   format(X,'trsw',$)
      imode=0
      call onrec(imode)
      RETURN
      END
```

```
      subroutine IBDAT(OFFSET,aGAIN,NCOUNT)

      COMMON /BLK1/IDATA(260)/GAINER/UPDOWN
      logical*1 messag(50)
      integer updown
      REAL*8 DATA,adata,bdata,cdata,offset,again

      updown=1
      ISTAT=IBSTS(1)
      ISTAT=IBSTS(1)
      IF((ISTAT.AND."1).EQ.1)call IBGAIN !channel A overload
      call ibget(1)
      N=IBRECV(messag,50,1)
      decode (20,98,messag)adata,bdata
      if (adata.lt.0.9)updown=-1
      if (updown.eq.-1) call ibgain
1     CALL IBSDC(1)          !CLEARS THE 385-EO FOR NEXT READING
      CALL IBGET(1)          !TRIGGERS THE 385-EO TO TAKE A
C                            !READING
      N=IBRECV(messag,50,1)    !GET DATA (samp,ref ASCII FORM)
      decode (20,98,messag)adata,bdata
98    format(2D19.10)
      cdata=adata/bdata
      IF(CDATA.GT.0.0D0)DATA = DLOG10(cdata)
      IF(CDATA.LT.0.0D0)DATA = -DLOG10(DABS(cdata))
      IF(CDATA.EQ.0.0D0)TYPE *,'RATIO IS ZERO ----
      1                        SOMETHING IS WRONG'
      IF(CDATA.EQ.0.0D0)DATA = 0.0
C
      IDATA(NCOUNT) = DATA * aGAIN      !4096=0.v  DAC OUTPUT
C                                       !0000=10.v DAC OUTPUT
C                                       ! F.S. OD  | aGAIN
C                                       !-------------------
C                                       !     .25  | 16384
C                                       !     .5   |  8192
C                                       !     1.   |  4096
C                                       !    1.5   |  2731
C                                       !     2.   |  2048
C                                       !     3.   |  1024
C
      IOUT = (4096 - IDATA(NCOUNT) + (OFFSET*aGAIN))
      CALL IPOKE("170442,IOUT) !NEWEST VALUE OUTPUT TO DAC(1)
      RETURN
      END
```

```
      SUBROUTINE PEN
C
C     USE DAC CHANNEL 3 BIT 4 (+5v)
C
      CALL ipoke("170440,"4000)
      DO 700 J=1,375
         K=J+1
700      CONTINUE
      CALL ipoke("170440,"7777)
      RETURN
      END
```

```
      SUBROUTINE IBGAIN

c     This routine is entered if the Ithaco 385E0 senses an
c     overload or if the reference lock-in output is < 0.09v.
c     It then determines what the 397E0 LIA gain settings are
c     and changes them by a factor of ten. The routine then
c     waits 10 seconds for the time constants to settle on
c     the new readings.

      integer updown
      common/gainer/updown
      logical*1 MESSAG(50),nessag(3)

      messag(1)=63   ! 63 = '?' gets 385E0 to ready parameters
      message(2)=13  ! 13 = 'CR' end of message
      nessag(1)=71   ! 71 = 'G' character controlling LIA gain
      nessag(3)=13   ! 13 = 'CR' end of message
      CALL IBSEOI(messag,2,1)           ! send '?CR' to 385E0
      CALL IBRECV(MESSAG,50,1)          ! receive parameters
      do 10 i=1,50                      ! find the 'G'
      if(messag(i).eq."107)go to 20     ! in the
10    continue                          ! parameter string
20    nessag(2)=(messag(i+1)+updown)    ! +/- 1 to the digit
C                                       !after the 'G'

      if(nessag(2).eq.0.or.nessag(2).eq.7)go to 30

      call ibseoi(nessag,3,1) !send modified gain code:'Gn'
      call isleep(0,0,10,0)    ! wait 10 s for RC to settle
      return
30    type *,'computer attempt to set LIA
      1        gain past limits of operation'
      return
      END
```

```
      SUBROUTINE ONREC(IMODE)
C
C
      IF(IMODE.EQ.0)GO TO 1000
C
C
C     THE FIRST ROUTINE SETS THE VISUAL 102 TO PRINTER
C     CONTROLLER MODE SEE THE OWNERS MANUAL FOR MORE
C     INFORMATION

      ib=27
      ic=91
      id=53
      ie=105
      write(7,101)ib,ic,id,ie
101   format(X,4a1,$)
      RETURN
C
C
C       THIS ROUTINE RESETS THE TERMINAL TO NORMAL STATUS
C
C
1000  id=52
      write(7,101)ib,ic,id,ie
      RETURN
      END
```

```
      SUBROUTINE YORN
C
C     SUBROUTINE YORN LOOKS FOR A CONSOLE RESPONSE
C     TO A YES-OR-NO QUESTION.  IF RESPONSE BEGINS
C     WITH 'Y' A VALUE OF 1 IS RETURNED IN JANSR;
C     IF WITH AN 'N,' A 0 IS RETURNED.
C
      common/sub1/jans
      LOGICAL*1 ANSWER(20)
      jans=0
10    READ (5,11) ANSWER
11    FORMAT (20A)
      IF (ANSWER(1).EQ.'Y')GO TO 13
      IF (ANSWER(1).EQ.'N')GO TO 14
      WRITE (7,12)
12    FORMAT (X,'GIVE YES OR NO RESPONSE: ',$)
      GO TO 10
13    jans=1
14    RETURN
      END
```

```
      SUBROUTINE SPACE

      IMODE=1
      call onrec(imode)
      WRITE(7,101)
  101 FORMAT(X,'tq12',$)
      imode=0
      call onrec(imode)
      call isleep(0,0,3,0)
      IMODE=1
      call onrec(imode)
      WRITE(7,102)
  102 FORMAT(X,'3333',$)
      imode=0
      call onrec(imode)
      return
      end
```

```
      PROGRAM GROWTH

C     THIS PROGRAM COLLECTS DATA WHILE THE LASER IS BURNING A
C     HOLE. THIS SHOULD ENABLE THE MONITORING OF HOLE GROWTH.

      IMPLICIT REAL (A-H,O-Z)
      DIMENSION SUM(3000),ISUM(3000)

C     INITIALIZE DATA ARRAY

      DO 20 I=1,3000
         SUM(I) = 0.0
20       CONTINUE

      TYPE *,'ENTER 1 IF YOU WANT TO MEASURE
     1        HOLE GROWTH FOR 17 MIN'
      TYPE *,'ENTER 2 IF YOU WANT MORE TIME'
      ACCEPT *,LEN
      IF (LEN .EQ. 1) GOTO 500
      TYPE *,'HOW LONG DO YOU WANT TO BURN (165 MIN MAX) ?'
      ACCEPT *,BTIM

C     JTIM IS AN INTEGER VALUE EQUAL TO THE NUMBER OF MINUTES
C     CHOSEN FOR BURNING

      JTIM = ((BTIM*60.)-1000.)/10.

C     DAOUTP IS A MACRO ROUTINE WHICH SENDS A
C     SIGNAL TO THE DESIRED D/A CONVERTER CHANNEL, THE FIRST
C     VARIABLE.  THE SIGNAL LEVEL IS DETERMINED BY THE SECOND
C     VALUE.  THE D/A CONVERTERS ARE SET UP AS EITHER
C     BIPOLAR, ±10 VOLTS, OR UNIPOLAR, 0 TO 10 VOLTS.  IN
C     BOTH CASES, A VALUE OF 4096 IS THE MINIMUM OUTPUT
C     VOLTAGE AND A VALUE OF 0 IS THE MAXIMUM VOLTAGE.

500   CALL DAOUTP(3,3072)       !SEND A -5V SIGNAL TO THE LASER
      CALL DAOUTP(4,4)          !OPEN THE SHUTTER
      PAUSE 'PRESS RETURN WHEN ALIGNED'
      CALL DAOUTP(4,0)          !CLOSE THE SHUTTER
      CALL DAOUTP(3,2048)       !SEND 0 VOLTS TO THE LASER

      PAUSE 'PRESS RETURN WHEN READY TO BEGIN'
      CALL DAOUTP(4,4)          !OPEN THE SHUTTER
      DO 10 I=1,1000
5        CALL AREADP(ISTAT,IBUFF0,1,0)!READS ADC 0
         CALL AREADP(ISTAT,IBUFF1,1,1)!READS ADC 1
         IF (IBUFF1 .EQ. 0) GOTO 5     !CHECK FOR SIGNAL
         SUM(I) = ((FLOAT(IBUFF0)/FLOAT(IBUFF1))*10000)
```

```
        CALL ISLEEP(0,0,0,6)            !WAIT FOR 1/10 SEC
10      CONTINUE
    DO 110 I=1,900
15      CALL AREADP(ISTAT,IBUFF0,1,0)!READS ADC 0
        CALL AREADP(ISTAT,IBUFF1,1,1)!READS ADC 1
        IF (IBUFF1 .EQ. 0) GOTO 15    !CHECK FOR SIGNAL
        SUM(I+1000) = ((FLOAT(IBUFF0)/FLOAT(IBUFF1))*10000)
        CALL ISLEEP(0,0,1,0)          !WAIT FOR 1 SEC
110     CONTINUE
    IF (LEN .EQ. 1) GOTO 501
    DO 210 I=1,JTIM
25      CALL AREADP(ISTAT,IBUFF0,1,0)!READS ADC 0
        CALL AREADP(ISTAT,IBUFF1,1,1)!READS ADC 1
        IF (IBUFF1 .EQ. 0) GOTO 25    !CHECK FOR SIGNAL
        SUM(I+1900) = ((FLOAT(IBUFF0)/FLOAT(IBUFF1))*10000)
        CALL ISLEEP(0,0,10,0)         !WAIT FOR 10 SEC
210     CONTINUE
501 CALL DAOUTP(4,0)                  !CLOSE SHUTTER
    CALL DAOUTP(3,3072)               !RESET LASER
    DO 30 I=1,3000
        ISUM(I)=SUM(I)   !CONVERT REAL NUMBER DATA TO INTEGER
30      CONTINUE
    CALL WRTDAT(ISUM)    !SUBROUTINE TO WRITE OUTPUT
    END
```

X. APPENDIX B: FORTRAN COMPUTER PROGRAMS FOR DATA ANALYSIS

```
      PROGRAM GROWTH

C     This routine evaluates Eq. 7 for user input values of
C     λ0, σ2 and S.  In addition, the experimental conditions
C     must be input by the user.  The output is stored in an
C     ascii file for plotting at a later time.

      IMPLICIT REAL*4 (A-H,O-Z), INTEGER*2 (I-N)
      DIMENSION T(1000),Y(1000),X(1000),WT(1000)
      CHARACTER*30 NAMF
      COMMON /THEO/ AL0,S2,TAU
      COMMON /CONT/ PLANCK,SOL,OMEGA,VAL
      EXTERNAL FX

      DO 10 I=1,1000          ! Initialize variables
            T(I)=0.0          ! Time
            X(I)=0.0          ! Integration variable
            WT(I)=0.0         ! Weights for Bode's Rule
10          Y(I)=0.0          ! Data values

      PLANCK=6.626196E-34 ! Planck's constant
      SOL=2.9979E10       ! Speed of Light
      OMEGA=1.0E12        ! Ω0
      CORR=1.0            ! S correction

      READ (5,*) TMIN,TMAX,NP      ! Range of times desired
      RANGE=ALOG10(TMAX)-ALOG10(TMIN)
      DO 30 I=1,NP
         AINDEX=(I-1)*(RANGE/NP)
30       T(I)=10.00**AINDEX*TMIN

      READ (5,*) AINTEN,BLAMB,SIGMA,ALIFE  ! IB, λB, σ and k
      READ (5,*) AL0,S2,SR                 ! λ0, σ2 and S
      VAL=AINTEN*SIGMA*OMEGA*BLAMB/(PLANCK*SOL*ALIFE)  ! Σ0
      CORR=1-EXP(-SR)                      ! S correction
      XCORR=CORR/(1-CORR)

      DO 50 I=1,NP
         TAU=T(I)
         B=(ALOG(50/(TAU*VAL))+2*AL0)/(2*S2)   !upper limit
         A=-10.                                !lower limit
         NINT=62                          !number of intervals
         CALL BODE(A,B,NINT,X,WT)         !Bode's Rule
         SUM=0.0
         DO 60 J=1,NINT*4+1
60          SUM=SUM+WT(J)*FX(X(J))
50       Y(I)=SUM/2.5066282750            !Divide by √2π
```

```
      READ (5,101) NAMF                    !Output file name
      OPEN (UNIT=9,FILE=NAMF)
      DO 70 I=1,NP
         pnt=0.0
         pnt=(y(i)/y(1)+xcorr)/(1+xcorr)   !Normalization
70       WRITE (9,113) T(I),pnt

101   FORMAT (A)
113   FORMAT (2F10.4)

      STOP
      END
```

```
      SUBROUTINE BODE(A,B,NINT,X,WT)

C     This subroutine integrates a user supplied function
C     using Bode's Rule [67].

      IMPLICIT REAL*4 (A-H,O-Z), INTEGER*2 (I-N)
      DIMENSION X(1000),WT(1000)
      EXTERNAL FX

      XDIF=(B-A)/NINT/4                    !Interval size

      CN0=14./45                           !Weight initialization
      CN1=64./45
      CN2=24./45
      CN3=64./45
      CN4=14./45

      I=1
      X(I)=A
      DO 100 K=1,NINT
         WT(I)=CN0*XDIF
         I=I+1
         X(I)=X(I-1)+XDIF
           WT(I)=CN1*XDIF
         I=I+1
         X(I)=X(I-1)+XDIF
         WT(I)=CN2*XDIF
         I=I+1
         X(I)=X(I-1)+XDIF
         WT(I)=CN3*XDIF
         I=I+1
100      X(I)=X(I-1)+XDIF
      WT(I)=CN4*XDIF

      I=5
      DO 101 K=1,NINT-1
         WT(I)=WT(I)+CN4*XDIF
101      I=I+4

      RETURN
      END
```

```
      FUNCTION FX(Z)

C     This function is Eq. 7 of the text.

      IMPLICIT REAL*4 (A-H,O-Z), INTEGER*2 (I-N)
      COMMON /THEO/ ALO,S2,TAU
      COMMON /CONT/ PLANCK,SOL,OMEGA,VAL

      XP=EXP(-2*ALO+2*S2*Z)
      CONS=XP*VAL
      FX=EXP(-Z*Z*0.5)*EXP(-CONS*TAU)

      RETURN
      END
```